Abdelhameed *et al.*
*Future Journal of Pharmaceutical Sciences (2025) 11:149*
https://doi.org/10.1186/s43094-025-00907-2

Future Journal of Pharmaceutical Sciences

RESEARCH

Open Access

# Phytochemical and antiviral investigation of *Cynanchum acutum* L. extract and derived semi-synthetic analogs targeting SARS-CoV-2 main protease

Reda F. A. Abdelhameed[1,2†], Ahmed K. Ibrahim[1†], Khaled M. Darwish[3,4], Asmaa M. Atta[5], Sarah Shabayek[6], Mona Timan Idriss[7], Amany K. Ibrahim[1], Safwat A. Ahmed[1], Jihan M. Badr[1*], Asma Ahmad Nashawi[8], Samar S. A. Murshid[9], Manar O. Lashkar[10], Sameh S. Elhady[11*] and Eman S. Habib[1]

## Abstract

**Background** The genus *Cynanchum*, family Apocynaceae is a group of climbing vines that have long been in folk medicine used as antitussives, analgesics, anticonvulsants, expectorants, diuretics, antifebriles, and tonics.

**Results** *Cynanchum acutum* crude extract was investigated to determine its chemical composition through LC-ESI-TOF-MS/MS technique, where 46 hits were observed. Among these compounds, quercetin-3-*O*-*β*-galactoside was previously reported within the plant as a major component. This compound was isolated and purified using different chromatographic techniques, and its concentration was estimated using high-performance thin-layer chromatography (HPTLC). Two semi-synthetic derivatives were synthesized from this compound, namely 7-benzyl- and 7-bromoethyl quercetin-3-*O*-*β*-galactosides. Both analogs, which are more hydrophobic, were developed as an attempt to improve the physiochemical properties and, in turn, the pharmacokinetics of the parent compound. Our study also includes the determination of antiviral activity against COVID-19 of *Cynanchum acutum* crude extract along with quercetin-3-*O*-*β*-galactoside in addition to the two semi-synthesized derivatives. The antiviral assay revealed that the synthetic benzyl derivative of quercetin-3-*O*-*β*-galactoside demonstrated promising activity against severe acute respiratory syndrome coronavirus 2 (SARS-CoV-2). The potential molecular aspects of the parent and semi-synthetic analogs were highlighted through molecular modeling simulation of docking the compounds at the viral main protease (Mpro) binding pocket. In silico findings demonstrated significant affinity and residue-wise binding interactions in relation to the co-crystallized small molecule Mpro inhibitor.

**Conclusion** Collectively, our study adds to the current knowledge of SARS-CoV-2 pharmacotherapy by introducing drug-like small molecules with potential activity profiles.

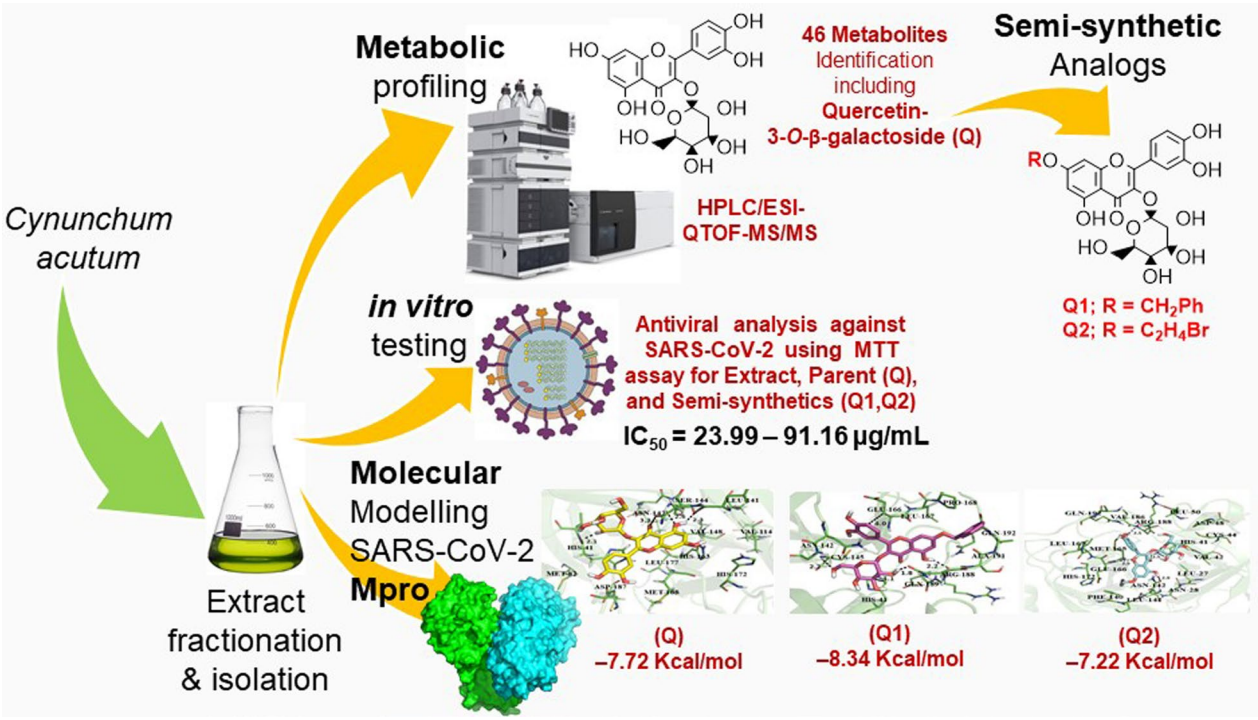
**Keywords** *Cynanchum acutum*, LC–MS/MS, Antiviral, COVID-19, SARS-CoV-2, Molecular modeling

†Reda F. A. Abdelhameed and Ahmed K. Ibrahim have contributed equally to this work and share first authorship.

*Correspondence:
Jihan M. Badr
gehan_ibrahim@pharm.suez.edu.eg
Sameh S. Elhady
ssahmed@kau.edu.sa
Full list of author information is available at the end of the article

© The Author(s) 2025, corrected publication 2025. **Open Access** This article is licensed under a Creative Commons Attribution 4.0 International License, which permits use, sharing, adaptation, distribution and reproduction in any medium or format, as long as you give appropriate credit to the original author(s) and the source, provide a link to the Creative Commons licence, and indicate if changes were made. The images or other third party material in this article are included in the article's Creative Commons licence, unless indicated otherwise in a credit line to the material. If material is not included in the article's Creative Commons licence and your intended use is not permitted by statutory regulation or exceeds the permitted use, you will need to obtain permission directly from the copyright holder. To view a copy of this licence, visit http://creativecommons.org/licenses/by/4.0/.

**Graphical abstract**




## Introduction

The *Cynanchum* genus is a group of climbing vines that previously belonged to the family Asclepiadaceae (milkweed family) but is now categorized under the family Apocynaceae. In folk medicine, plants in the genus *Cynanchum* have long been used as antitussives, analgesics, anticonvulsants, expectorants, diuretics, antifebriles, and tonics [1].

The climbing vine *Cynanchum acutum* L. is indigenous to Asia, Africa, and Europe. It grows widely in Egypt, and native Egyptians refer to it as "*ollig*," "*modeid*," or "*libbein*" [2, 3]. There have been reports of antioxidant [4], anticancer [5], antidiabetic [4], antibacterial [6], insecticidal [7], antipyretic, analgesic, and anti-inflammatory [6] properties of the alcoholic leaves' extract of *C. acutum*. Additionally, *C. acutum* extract showed a preventive action against hepatotoxicity induced by carbon tetrachloride in rat models [8]. The genus *Cynanchum* was also reported for its antiviral activities [9, 10]. The phytochemical investigation of *Cynanchum* plants showed that *Cynanchum* plants are rich in phytochemicals, such as carbohydrates [11], triterpenes [12], esters of long-chain fatty acids [13], alkaloids [14], coumarins [15], and flavonoids [16].

Despite the World Health Organization (WHO) announcing the end of the COVID-19 pandemic, the infection of this virus is still beyond control due to the emergence of new virulent variants that kept spreading causing reinfections worldwide [17]. As for now, there are more than 1000 recorded variants of SARS-CoV-2, including the prominent epidemic variants, Beta, Delta, and Omicron [18]. The Food and Drug Administration (FDA) approved Veklury (remdesivir) is primarily used for treating severe COVID-19 cases in those who have mild-to-moderate COVID-19, hospitalized or not, and are at high risk for developing severe COVID-19, which might result in hospitalization or death [19]. Paxlovid (nirmatrelvir and ritonavir) and Lagevrio (molnupiravir) are FDA-approved but permitted under the authorization of emergency use (EUA) for certain patients [19]. Moreover, the FDA-approved COVID-19 vaccines are of limited efficacy in stimulating the innate immune response against infections induced by the recently appearing SARS-CoV-2 variants [20, 21]. Consequently, finding efficient therapeutic treatments for COVID-19 is crucial during the early symptomatic stage of the illness. Exploring potential and efficacious phytochemicals that function as phytomedicines represents a promising strategy to address global requirements.

The current study aimed to define the phytochemical profile and assess the antiviral efficacy of the crude extract of *C. acutum* as well as quercetin-3-*O*-*β*-galactoside (as a major constituent of the plant) together with two synthesized derivatives against COVID-19.

## Materials and methods

### Plant material and the extraction process

Samples of the entire plant of *C. acutum* were meticulously gathered from three distinct horticultural sites at the University of Suez Canal: the Garden of the Faculty of Pharmacy, the Garden of the Faculty of Commerce, and the Garden of the Faculty of Nursing in October, 2019. The botanical identification of the plants specimen was validated by Professor Sayeda Gamal Eldin, Professor of Botany at the Faculty of Science, Suez Canal University. The specimen designated as #SAA-157 was archived in the herbarium lab of the Pharmacognosy Department within the Faculty of Pharmacy at Suez Canal University, Egypt. The extraction procedure was conducted in accordance with the previously outlined methodology [22], as follows: The harvested plant specimen, weighing 10 kg, was subjected to a drying process, subsequently ground into a fine powder, and extracted using methanol (4×5 L). The resultant yield was then concentrated under reduced pressure utilizing a rotary evaporator, culminating in the production of 531 g of the methanolic extract.

### LC–MS-MS of the crude extract of *Cynanchum acutum*

#### *Sample preparation*

Fifty milligrams of *Cynanchum acutum* crude extract was solubilized in one milliliter of a mobile phase working solution (MP-WS), which consisted of distilled water, methanol, and acetonitrile in a volumetric ratio of 50:25:25. The solution was subjected to vortex mixing for a duration of two minutes, followed by ultrasonication for a period of ten minutes. The sample was then centrifuged for ten minutes at 10,000 Revolutions Per Minute (rpm) to yield a stock solution. A volume of 20 µL of the stock solution (50/1000 µL) was further diluted using 1000 µL of reconstitution solvent to reach a final concentration of 1 µg/µL. An aliquot of 10 µL of the freshly prepared sample was injected in both ionization modes, positive and negative, while an additional 10 µL of the reconstitution solvent (MP-WS) was injected to be used as a blank to ensure the reliability of the results [23]. The employed mobile phases were calibrated as follows: (A) for the positive ionization mode, a five millimolar ammonium formate buffer at pH 3 incorporating 1% methanol; (B) for the negative ionization mode, a five millimolar ammonium formate buffer at pH 8 comprising 1% methanol; (C) for both ionization modes (positive and negative), 100% acetonitrile was utilized. The pre-column utilized was an in-line filter disk (Phenomenex, 0.5 µm×3.0 mm), while the analytical column was an X select HSS T3 (Waters, 2.5 µm, 2.1×150 mm), and the flow rate was maintained at 0.3 mL/min with a constant column temperature equal to 40 °C. The gradient system was configured as follows:Time/% A (or B)/% C: 0/90/10, 1/90/10, 21/10/90, 25/10/90, 25.01/90/10, 28/90/10.

#### *Data processing*

Data were analyzed utilizing MS-DIAL version 3.52. The MasterView software facilitated the extraction of features (peaks) of the total ion chromatogram (TIC) based on specific criteria: For non-targeted analysis, features were required to exhibit a signal-to-noise ratio exceeding 5 and sample-to-blank intensities surpassing 5. The identification of compounds was achieved through precise mass calculations, MS/MS transitions, and the retention time comparison of compounds with data documented in the existing literature, as well as in mass spectrum databases pertinent to LC/MS-based metabolomic studies (databases employed: ReSpect negative (1573 records) and positive (2737 records).

### Isolation and identification of the major compound (quercetin-3-*O*-*β*-galactoside)

Among the major phytochemicals identified in the crude extract of *the Cynancum acutum* plant, quercetin-3-*O*-*β*-galactoside was previously isolated and identified as reported in [22]. Accordingly, we followed the same procedure for the isolation and purification of the compound as the following: The dried crude extract of *Cynancum acutum* (531 g) was suspended in 1.5 L of distilled water, subsequently undergoing successive extractions with 4 L each of *n*-hexane, chloroform, ethyl acetate, and butanol. Each of the four extracts was dried under vacuum using a rotary evaporator. The ethyl acetate dried extract (62 g) was fractionated using an *n*-hexane/ethyl acetate gradient until 100% ethyl acetate, followed by an ethyl acetate/methanol gradient until 100% methanol. The fraction eluted using 35% methanol in ethyl acetate (1.5 g) was subjected to column chromatography using a chloroform/methanol gradient until 100% methanol, followed by a methanol/water gradient until 10% water/methanol. Similar subfractions were monitored by thin-layer chromatography (TLC), pooled together, and evaporated to dryness to afford the purified major compound (quercetin-3-*O*-*β*-galactoside, 630 mg). Subsequently, the identification of the compound was confirmed by

co-chromatography with the reference quercetin-3-*O*-*β*-galactoside [22]. Moreover, the purity of the isolated compound was confirmed by the reversed-phase high-performance liquid chromatography (HPLC) method using the Young Line HPLC system model YL9100 (YL Instrument CO., Ltd., South Korea), equipped with a YL9101 vacuum degasser, a quaternary pump (model YL9110), a 20-l sample loop injector, and a YL9120 UV/Vis detector. Data acquisition was performed on Clarity software (version 7.00.258). Separation and quantitation were made on a Nucleodur 125×4 mm (i.d.) and 5-*μ*m particle-size reversed-phase C18 analytical column (Macherey–Nagel, Germany). An HPLC column oven was used, DALIAN REPLETE®, Hong Kong. The samples were injected with a 25-*μ*L Hamilton analytical syringe. The injection volume was 20 *μ*L. Sample solution was prepared by dissolving 1 mg of the isolated Quercetin-3-*O*-*β*-galactoside in 10 mL of methanol to get a solution containing 100 µg/mL. The isocratic mobile phase system giving satisfactory results was acetonitrile:water (14:86, v/v) and UV detection at 255 nm. The flow rate was adjusted at 0.2 mL/min, and the column temperature was kept at 25 °C. As a result, quercetin-3-*O*-*β*-galactoside was eluted as a pure singlet peak at 3.507 min (Fig. S1), confirming the purity of the isolated compound.

## HPTLC analysis

### *Instrumentation*

In accordance with the stipulations set forth by the International Council on Harmonization (ICH) guidelines [24], various concentrations of the methanolic solution of quercetin-3-*O*-*β*-galactoside were administered utilizing A CAMAG® (Muttenz, Switzerland) Linomat V, which was controlled with CAMAG winCats™ software version 1.4.4 (CAMAG, Muttenz, Switzerland). A 20 cm×10 cm silica gel plate 60 F254 (Merck™, Darmstadt, Germany) was employed. The experimental conditions were calibrated as follows: a slit dimension of 6 mm in length and 0.1 mm in width, an inter-track distance of 10.5 mm, with both the x-axis and y-axis distances maintained at 10 mm, and an application rate equal to 15 µL/second. The methanolic solutions were applied in duplicate. The development of quercetin-3-*O*-*β*-galactoside has been previously reported in the literature [25], where the compound was analyzed using reversed-phase TLC with a specific mobile phase. In the present study, we modified the method by employing normal-phase TLC and using a solvent mixture of ethyl acetate, formic acid, acetic acid, and water at a volumetric ratio of 100:11:11:26 (v/v/v/v, respectively) as the mobile phase to optimize separation under our experimental conditions. The development of the plates occurred within a twin-trough chamber that was saturated with the selected mobile phase. Development was conducted subsequent to a saturation period lasting 20 min. Following a development duration of 15 min, the plates underwent air-drying, after which the retention factor (Rf) was calculated. The spots were successfully separated with an appropriate Rf value of 0.60 ± 0.05. The quantification process was executed utilizing a CAMAG TLC Scanner III densitometer in conjunction with CATS version 4 X software, employing the absorption mode powered by a deuterium light source. Quantification was carried out at various wavelengths of λ = 256, 270, and 350 nm. The wavelength that exhibited optimal validation parameters (λ = 350 nm) was used for the formulation of the calibration curve.

*Chemicals* Standard quercetin-3-*O*-*β*-galactoside was extracted from the plant and purified as described [22]. The solvents (ethyl acetate, formic acid, acetic acid, water, and methanol) utilized for dissolution and development, along with the pre-coated silica gel F254 (0.25 mm), were obtained from Merck Company located in Darmstadt, Germany.

*Standard solution* A precise quantity of 20 mg of the standard quercetin-3-*O*-galactoside (Q) (Fig. 1) was accurately weighed for the purpose of preparing the standard stock solution. Subsequently, the solution was quantitatively transferred into a volumetric flask (10 mL), and the volume was meticulously adjusted with methanol to get a stock solution (A) of concentration 2 µg/µL. The stock solution A was kept in a refrigerator and securely sealed until its application in the construction of the calibration curve.

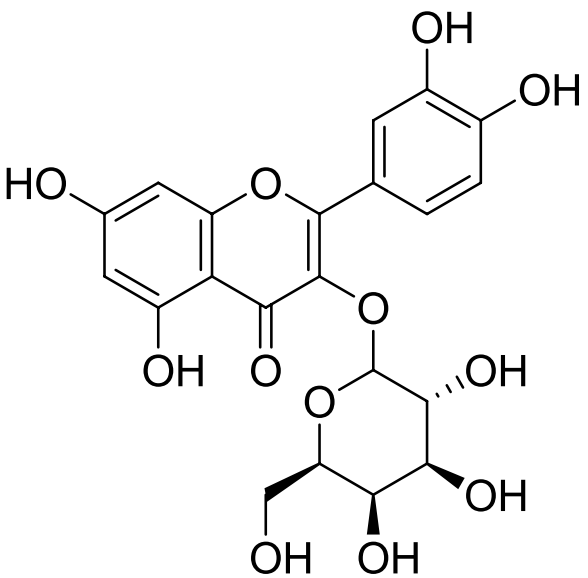



**Fig. 1** Quercetin-3-*O*-*β*-galactoside

*Sample preparation* An accurate amount of the dry crude plant extract (500 mg) was quantitatively transferred into a 10-mL volumetric flask, and the volume was adjusted using methanol. The resultant solution was stored in the refrigerator for subsequent experimental application.

*Calibration graph* The ICH criteria [24] were followed in the construction of the calibration curve. Different concentrations were applied to a (20 cm × 10 cm) plate, each in duplicate. Several solvent systems were tested for development, for instance, chloroform:methanol:water :acetic acid (7:3:0.5:0.1, v/v/v/v) and (6:3:1:0.1, v/v/v/v), chloroform:methanol (9:1, v/v), and ethyl acetate:formic acid:acetic acid:water (100:11:11:26, v/v/v/v). The solvent mixture consisting of ethyl acetate:formic acid:acetic acid:water (100:11:11:26, v/v/v/v) was found to be the optimum option, as it produced homogeneous compact bands with appropriate RF. After a saturation period of 20 min, development took place for 15 min, and 10 min for air-drying. Rf was determined to be 0.60 + 0.05.

### Preparation and purification of semi-synthetic derivatives of quercetin-3-*O*-*β*-galactoside (Q1-Q2)

#### *Chemistry*

Chemical reagents as well as solvents were sourced from commercial suppliers. In the case of reactions sensitive to air and moisture, dimethylformamide solvent underwent drying using Fisher molecular sieves of type 4A grade 514 (8–12 mesh; with an effective pore size of 4 Å) and was maintained under nitrogen, and the solution was transferred via a syringe and subsequently introduced into reaction vessels through rubber septa (Aldrich Sure/Seal). The progress of the reaction was assessed through thin-layer chromatography (TLC) using Merck silica gel 60 F254 plates. Visualization was conducted using ultraviolet light at a wavelength of 254 nm. Purification was performed using flash column chromatography on Loba Chemie silica gel (200–400 mesh) serving as a stationary phase. The yields reported correspond to purified compounds and were not optimized. Structure elucidation was proceeded through recording the $^{1}$H- and $^{13}$C nuclear magnetic resonance spectra (NMR) in hexadeuterodimethyl sulfoxide (DMSO-$d_6$) on a Bruker Ascend Aeon 400 spectrometer ($^{1}$H-NMR 400/500 MHz and $^{13}$C-NMR 101 MHz) at ambient temperature within the range of 20–25 °C. Using tetramethylsilane as the internal standard, chemical shifts (δ) are represented as parts per million (ppm) and were referenced to the corresponding residual solvent or deuterated solvent peaks.

#### *Synthesis of the benzyl derivative of quercetin-3-O-β-galactoside; 7-(benzyloxy)-2-(3,4-dihydroxyphenyl)-5-hydroxy-3-(((3R,4S,5R,6R)-3,4,5-trihydroxy-6-(hydroxymethyl) tetrahydro-2H-pyran-2-yl) oxy)-4H-chromen-4-one (Q1)*

To a solution of quercetin-3-*O*-*β*-galactoside (Q, 0.22 mmol) in dried dimethylformamide (DMF) (3 mL) at a temperature of 0 °C, potassium carbonate (0.24 mmol) was incrementally incorporated into the reaction mixture. The resulting mixture was subjected to stirring for a duration of 0.5 h at ambient temperature, subsequent to which benzyl bromide (0.24 mmol) was introduced dropwise. The reaction mixture underwent reflux with continuous stirring for a period of 12 h. The resultant reaction mixture was subjected to extraction using ethyl acetate, followed by the drying of the organic layer over magnesium sulfate and concentration under reduced pressure, yielding an oily brown residue. The purification process was executed through flash silica gel column chromatography utilizing a stepwise gradient elution (*n*-hexane/ethyl acetate; 80% *n*-hexane to 40%). The final compound was obtained as an orange oily residue. Yield: 85%. $^{1}$H-NMR (400 MHz, DMSO-d6) $\delta$ ppm 3.68 (br. s., 2 H, H-6′′), 5.26 (d, $J$ = 6.60 Hz, 2 H, H-1‴), 5.39 (br. s., 1 H, H-1″), 6.49 (d, 1 H, H-6), 6.84 (s, 1 H, H-2′), 7.14 (m, 1 H, H-8), 7.33–7.63 (m, 7 H).

#### *Synthesis of the bromoethyl derivative of quercetin-3-O-β-galactoside; 7-(2-bromoethoxy)-2-(3,4-dihydroxyphenyl)-5-hydroxy-3-(((3R,4S,5R,6R)-3,4,5-trihydroxy-6-(hydroxymethyl) tetrahydro-2H-pyran-2-yl) oxy)-4H-chromen-4-one (Q2)*

In a solution consisting of quercetin-3-*O*-*β*-galactoside (Q, 0.22 mmol) in dried DMF maintained at 0 °C, sodium hydride (0.24 mmol) was introduced gradually. The resulting mixture was stirred for a duration of 30 min at room temperature. Subsequently, 1-bromo-2-chloroethane (0.24 mmol) was added, and the resulting mixture was stirred at room temperature for an extended period overnight. The reaction mixture was then subjected to extraction using ethyl acetate, after which the organic phase was dried over magnesium sulfate and concentrated under reduced pressure, yielding a dark yellow residue. Purification was performed via silica gel column chromatography with stepwise gradient elution (*n*-hexane/ethyl acetate; 80% *n*-hexane to 40%). The final compound was obtained as a pale oily residue. Yield: 83%. $^{1}$H-NMR (500 MHz, DMSO-d6) $\delta$ ppm 3.28 (d, 1 H, H-6′′), 3.56 (dd, 1 H, H-6′′), 3.98 (m, 2 H, H-1‴), 4.31 (m, 2 H, H-2‴), 5.42 (ddd, 1 H, H-1′′),6.24 (m, 1 H, H-6), 6.44 (m, 1 H, H-8), 6.84 (m, 1 H, H-5′), 7.57 (d, 1 H, H-2′), 7.70 (dd, 1 H, H-6′).

## Determination of antiviral activity

### *The tested compounds*

The compound quercetin-3-*O*-$\beta$-galactoside (Q) was isolated and purified, and two derivatives were synthesized (Q1 and Q2). The three pure compounds (Q, Q1, and Q2) were subjected to antiviral analysis along with the MeOH crude extract of *C. acutum.*

### *The virus and the cell line*

Vero-E6 cells were cultured in Dulbecco's modified Eagle's medium (DMEM) supplemented with 10% fetal bovine serum (FBS) (Invitrogen) and 1% Penicillin/Streptomycin (pen/strep) antibiotic solution at a temperature of 37 °C in an atmosphere of 5% $CO_2$. The virus stock was generated by distributing Vero-E6 cells into tissue culture flasks 24 h prior to exposure to the Human Coronavirus-19 (hCoV-19/Egypt/NRC-3/2020) strain at a multiplicity of infection (MOI) of 0.1 in DMEM containing 2% FBS, 1% pen/strep, and 1% L-1-tosylamido-2-phenylethyl chloromethyl ketone (TPCK)-treated trypsin (the infection medium). The hCoV-19/Egypt/NRC-03/2020 strain (Accession Number on GSAID: EPI_ISL_430820) was graciously supplied by the Vaccine Development and Virological Tests Unit, Center of Scientific Excellence for Influenza Viruses, National Research Centre, Giza, Egypt.

### *MTT cytotoxicity assay*

The 3-(4, 5-dimethylthiazol -2-yl)-2,5-diphenyltetrazolium bromide (MTT) method was employed to assess half maximal cytotoxic concentration ($CC_{50}$) in VERO-E6 cells as delineated by [26]. In summary, stock solutions of test compounds were prepared in 10% dimethyl sulfoxide (DMSO) in double-distilled water ($ddH_2O$). These were subsequently diluted to working solutions with DMEM. VERO-E6 cells were plated in 96-well plates (100 µl/well) at a concentration of $3\times10^5$ cells/ml and were incubated for a duration of 24 h at 37 °C in an atmosphere containing 5% $CO_2$. Afterward, the cells underwent treatment with various concentrations of the compounds under investigation, conducted in triplicate. After a 24-h incubation period, the supernatant was removed, and cell monolayers were subjected to three washes with sterile 1 × phosphate-buffered saline (PBS). Thereafter, 20 $\mu$L/well of MTT solution (5 mg/mL) was introduced, and the cells were incubated at 37 °C for 4 h, after which the medium was aspirated. The resultant formazan crystals in each well were solubilized with 200 $\mu$L of acidified isopropanol (0.04 M HCl in absolute isopropanol). The absorbance of formazan solutions was measured at a wavelength of 540 nm with 620 nm as a reference wavelength. The cytotoxicity percentage in relation to untreated cells is assessed using the following equation:

% cytotoxicity = ((Absorbance of cells without treatment—Absorbance of cells with treatment) × 100)/(absorbance of cells without treatment).

The graphical representation of % cytotoxicity against sample concentration was employed to determine the concentration that induced 50% cytotoxicity ($CC_{50}$).

### *Determination of inhibitory concentration 50 (IC50)*

The inhibitory concentration was determined in accordance with the methodology outlined by [26]. Vero-E6 cells were dispensed into 96-well plates ($2.4\times10^4$ cells/well) and incubated overnight at a temperature of 37 °C in an atmosphere of 5% $CO_2$. Following this incubation period, the cell monolayers were rinsed with 1 × PBS and exposed to virus adsorption for a duration of one hour at room temperature. This was followed by further overlay with 100 µl of DMEM medium containing varying concentrations of the test compounds, maintained at 37 °C in 5% $CO_2$ for a period of 72 h. Then, cells were fixed for 20 min using 100 $\mu$L of 4% paraformaldehyde and subsequently stained with 0.1% crystal violet for 15 min at room temperature. The crystal violet was then solubilized using absolute methanol (100 $\mu$L/well), and the optical density of the obtained color was quantified at a wavelength of 570 nm. The $IC_{50}$ value of a compound is necessary to diminish the virus-induced cytopathic effect (CPE) by 50%, in comparison with the virus control.

## Docking analysis

The molecular docking workflow was carried out using AutoDock Vina V.1.2.0 (Scripps Research, La Jolla, CA, USA). The binding site was characterized by the co-crystallized ligand, and the docking was carried out using the Vina Forcefield and Lamarckian Genetics, with the biological target center serving as the center of the docking box. The global search exhaustiveness was established at 100 kcal $mol^{-1}$, whereas the maximal energy variation between poses was fixed at 3 kcal $mol^{-1}$.

The target proteins (8B56) were obtained from the Research Collaboratory for Structural Bioinformatics (RCSB) Protein Data Bank. The AutoDock Tool package v1.2.0 was utilized to structurally prepare the downloaded protein by eliminating co-crystallized ligand, solvent, and ions; incorporating polar hydrogen atoms and partial charges; and merging non-polar hydrogens absent from the X-ray crystallized Protein Data Bank (PDB) file [27]. The generated target proteins were subsequently transformed into Protein Data Bank, Partial charge (Q) & Atom type (T) (PDBQT) file format for subsequent utilization. Synthesized compounds were generated, transformed into 3D structures, energy-minimized using Assisted Model Building with Energy Refinement

(AMBER) partial charges/modified forcefield, and subsequently converted into PDBQT files utilizing the OpenBabel tool v.2.3.1 (National Supercomputer Centre, Linköping, Sweden).

## Results

### LC–MS/MS of *Cynanchum acutum*

By employing the sophisticated LC–MS/MS technique, an extensive metabolomic analysis of *Cynanchum acutum* extract was performed to investigate the diverse chemical components of its metabolites. Through the correlation of the *m/z* values of the precursors, the MS/MS fragment ions, and the retention times with those documented in existing literature, the individual constituents were provisionally ascertained. In this study, a total of 46 distinct phytochemicals were identified within the extract of *Cynanchum acutum* (Table 1, Fig. 2).

Twenty of the identified compounds were characterized as typical flavonoids (aglycones & glycosides). Among these, six were aglycones, including diosmetin, fisetin, kaempferide, kaempferol, naringenin, and quercetin, along with 14 glycosides, including four quercetin glycosides, three luteoline glycosides, three kaempferol glycosides, three isorhamnetines, datiscin, quercetrin, and rutin. These findings elucidate the abundance of flavonoids present in the extract derived from *Cynanchum acutum.* Nine of these compounds (Kaempferol, Kaempferol-3-*O*-glucoside, Luteolin-6-C-glucoside, Luteolin-7-*O*-glucoside, Quercetin, Quercetin 3-*O*-galactoside, Quercetin-3-D-xyloside, Quercetin-4'-glucoside, and rutin were found to be previously isolated from *Cynanchum acutum* [22, 28–31]. Thus, eleven of the identified flavonoids (datiscin, diosmetin, fisetin, isorhamnetin-3-glucoside, kaempferide, kaempferol-3,7-di-glucoside, kaempferol-3-*O*-rutinoside, luteolin-7-*O*-neohesperidoside, naringenin, quercetin-3,4'-*O*-di-beta-glucopyranoside, and quercetrin) can be considered as firstly reported from *Cynanchum acutum.*

## Discussion

### HPTLC analysis

#### *Linearity*

The assessment of the linearity of the HPTLC methodology was conducted by evaluating various concentrations of the standard quercetin-3-*O*-*β*-galactoside, with each concentration being applied in duplicate. The calibration curve data (scanned at $\lambda = 350$ nm) demonstrated a good linear correlation across the concentration spectrum of 100–1100 ng per band in relation to the area. The calculated correlation coefficient ($R^2$) was 0.989, and the derived linear regression equation was established as $y = 14.955x + 2342$, wherein $y$ denotes the spot area, and $x$ signifies the concentration of quercetin-3-*O*-*β*-galactoside.

#### *System precision*

The system precision was evaluated through the determination of a specified concentration (0.3 µg/band equivalent to 300 ng/band) of the reference quercetin-3-*O*-*β*-galactoside, which was also applied in duplicate. The resultant values of percent relative standard deviation (*%RSD*) were found to be 1.36 indicating the precision**.**

#### *Method precision*

This precision was further validated through the repeated analysis of the plant extract, which was scanned at $\lambda = 350$ nm. The sample was applied twice using the same previously described procedure. The minimal value of *%RSD* (1.91) underscored the methodological precision.

#### *Accuracy*

The accuracy of the proposed method was substantiated through the incorporation of a pre-analyzed sample into a standard quercetin-3-*O*-*β*-galactoside solution of known concentration, followed by the analysis of the fortified sample utilizing the same procedural approach. Upon conducting the analysis of the resultant mixture (executed in duplicate), the mean percentage recovery was calculated.

[(observed conc.—actual conc.)/ actual] *100.

The % recovery was found to be 97.71%.

#### *Limits of detection and quantification*

The determination of the limits of detection and quantification was predicated upon the subsequent equations: $3\ \sigma / S$ for the limit of detection and $10\ \sigma / S$ for the limit of quantification, where $\sigma$ represents the standard deviation of the response and $S$ denotes the slope of the calibration curve. Limit of detection (LOD) was calculated as 22 ng, while limit of quantification (LOQ) was found to be 70 ng.

#### *Analytical solution stability*

Analytical solutions of quercetin-3-*O*-*β*-galactoside in methanol were maintained at room temperature for a duration of 48 h. Upon the repetition of the experiment, no alterations were observed in the results, thereby suggesting the stability of the solutions. Furthermore, when subjected to refrigeration at a temperature of 4 °C for a period of up to 10 days, no variations in the results were identified, further indicating the stability of the solutions under these specified conditions.

**Table 1** LC–MS/MS metabolic analysis of *Cynanchum acutum* extract

| Polarity Mode | Ret. Time (Min.) | Observed *m/z* | Calculated *m/z* | Mass Error (ppm) | Adduct | Molecular formula | MS/MS spectrum | Deduced compound | Occurrence in *C. acutum* | References |
|---|---|---|---|---|---|---|---|---|---|---|
| Negative | 1.12 | 117.0183 | 117.0188 | −4.3 | $[M—H]^-$ | $C_4H_6O_4$ | 117, 73 | Succinic acid | Reported in other *Cynanchum* species | [32] |
| Negative | 1.16 | 133.0136 | 133.0137 | −0.8 | $[M—H]^-$ | $C_4H_6O_5$ | 133, 115, 71 | Malic acid | First report in *C. acutum* | [33, 34] |
| Negative | 1.18 | 195.0499 | 195.0505 | −3.1 | $[M—H]^-$ | $C_6H_{12}O_7$ | 195 | Gluconate | First report in *C. acutum* | [35] |
| Negative | 1.19 | 128.0347 | 128.0348 | −0.8 | $[M—H]^-$ | $C_5H_7NO_3$ | 130, 84 | L-5-Oxoproline (pyroglutamate) amino acid | First report in *C. acutum* | [36] |
| Negative | 1.26 | 289.0695 | 289.0712 | −5.9 | $[M—H]^-$ | $C_{15}H_{14}O_6$ | 289, 245 | (-)-Epicatechin | First report in *C. acutum* | [37] |
| Negative | 1.26 | 289.0695 | 289.0712 | −5.9 | $[M—H]^-$ | $C_{15}H_{14}O_6$ | 289, 245 | Catechin | Previously reported in *C. acutum* | [38] |
| Positive | 1.27 | 104.1066 | 104.1070 | −3.8 | $[M+H]^+$ | $C_5H_{14}NO$ | 104, 60 | Choline | First report in *C. acutum* | [39] |
| Positive | 1.31 | 118.0864 | 118.0868 | −3.4 | $[M+H]^+$ | $C_5H_{11}NO_2$ | 118, 58 | Glycine-Betaine | First report in *C. acutum* | [40] |
| Negative | 1.33 | 137.0234 | 137.0239 | −3.6 | $[M—H]^-$ | $C_7H_6O_3$ | 137, 93 | 4-hydroxybenzoic acid | Previously reported in *C. acutum* | [41] |
| Negative | 1.37 | 179.0551 | 179.0556 | −2.8 | $[M—H]^-$ | $C_6H_{12}O_6$ | 179, 89 | D-(-)-Tagatose-Monosaccharide | First report in *C. acutum* | [42] |
| Positive | 1.55 | 124.0392 | 124.0399 | −5.6 | $[M+H]^+$ | $C_6H_5N_2O_2$ | 124, 80 | Nicotinic acid | First report in *C. acutum* | [43] |
| Positive | 1.76 | 123.0554 | 123.0558 | −3.2 | $[M+H]^+$ | $C_6H_6N_2O$ | 123, 80 | Nicotinamide | First report in *C. acutum* | [44] |
| Negative | 1.77 | 163.0393 | 163.0395 | −1.2 | $[M—H]^-$ | $C_9H_8O_3$ | 163, 119 | *P*-coumaric acid | Previously reported in *C. acutum* | [45, 46] |
| Negative | 1.93 | 193.0499 | 193.0501 | −1.0 | $[M—H]^-$ | $C_{10}H_{10}O_4$ | 193, 178 | Ferulic acid | Previously reported in *C. acutum* | [47] |
| Negative | 4.61 | 609.1469 | 609.1456 | 2.1 | $[M—H]^-$ | $C_{27}H_{30}O_{16}$ | 447, 285 | Kaempferol 3, 7 di-glucoside | First report in *C. acutum* | [47] |
| Positive | 5.34 | 377.144 | 377.1461 | −5.6 | $[M+H]^+$ | $C_{17}H_{20}N_4O_6$ | 377, 243 | (-)-Riboflavin | First report in *C. acutum* | [48] |
| Negative | 5.54 | 609.1459 | 609.1456 | 0.5 | $[M—H]^-$ | $C_{27}H_{30}O_{16}$ | 609, 301, 300 | Rutin | Previously reported in *C. acutum* | [49–51] |
| Positive | 5.70 | 627.1596 | 627.1561 | 5.6 | $[M+H]^+$ | $C_{27}H_{30}O_{17}$ | 304.1, 303.04, 165.01, 85.03 | Quercetin-3,4′-*O*-di-glucopyranoside | First report in *C. acutum* | [52] |
| Positive | 5.76 | 138.055 | 138.0555 | −3.6 | $[M+H]^+$ | $C_7H_7NO_2$ | 138, 94, 92 | Trigonelline | First report in *C. acutum* | [43] |
| Negative | 6.13 | 593.1522 | 593.1506 | 2.7 | $[M—H]^-$ | $C_{27}H_{29}O_{15}$ | 593, 285 | Datiscin | First report in *C. acutum* | [53] |
| Negative | 6.13 | 593.1522 | 593.1506 | 2.7 | $[M—H]^-$ | $C_{27}H_{30}O_{15}$ | 593, 285 | Kaempferol-3-*O*-rutinoside | First report in *C. acutum* | [47, 54] |
| Negative | 6.13 | 593.1522 | 593.1506 | 2.7 | $[M—H]^-$ | $C_{27}H_{30}O_{15}$ | 593, 285.04 | Luteolin-7-*O*-neohesperidoside | First report in *C. acutum* | [55] |
| Positive | 6.19 | 611.1572 | 611.1607 | −5.7 | $[M]^+$ | $C_{27}H_{31}O_{16}{}^+$ | 611, 449, 287 | Cyanidin-3,5-di-*O*-glucopyranoside | First report in *C. acutum* | [56] |
| Positive | 6.19 | 303.0489 | 303.0505 | −5.3 | $[M+H]^+$ | $C_{15}H_{10}O_7$ | 303, 153 | Quercetin | Previously reported in *C. acutum* | [57] |

**Table 1** (continued)

| Polarity Mode | Ret. Time (Min.) | Observed *m/z* | Calculated *m/z* | Mass Error (ppm) | Adduct | Molecular formula | MS/MS spectrum | Deduced compound | Occurrence in *C. acutum* | References |
|---|---|---|---|---|---|---|---|---|---|---|
| Positive | 6.19 | 303.0485 | 303.0499 | −4.6 | $[M]^+$ | $C_{15}H_{11}O_7^+$ | 303, 257, 247, 229 | Delphinidin | First report in *C. acutum* | [58] |
| Negative | 6.42 | 191.0354 | 191.0344 | 5.2 | $[M—H]^-$ | $C_{10}H_8O_4$ | 191, 176 | Scopoletin | Previously reported in *C. acutum* | [59] |
| Negative | 6.51 | 433.0767 | 433.0771 | −0.9 | $[M—H]^-$ | $C_{20}H_{18}O_{11}$ | 433, 301, 300 | Quercetin-3-D-xyloside | Previously reported in *C. acutum* | [60] |
| Negative | 6.55 | 167.0349 | 167.0344 | 2.9 | $[M—H]^-$ | $C_8H_8O_4$ | 167, 152, 123, 108 | Vanillic acid | Previously reported in *C. acutum* | [45] |
| Negative | 6.57 | 447.0919 | 447.0927 | −1.8 | $[M—H]^-$ | $C_{21}H_{20}O_{11}$ | 447, 285 | Luteolin-7-*O*-glucoside | Previously reported in *C. acutum* | [61] |
| Negative | 6.57 | 447.0919 | 447.0927 | −1.8 | $[M—H]^-$ | $C_{21}H_{20}O_{11}$ | 447, 284 | Quercitrin | Previously reported in *C. acutum* | [51, 62] |
| Positive | 6.69 | 449.1071 | 449.1084 | −2.9 | $[M]^+$ | $C_{21}H_{21}O_{11}^+$ | 449, 287 | Cyanidin-3-glucoside | First report in *C. acutum* | [63–65] |
| Positive | 6.69 | 449.1071 | 449.1084 | −2.9 | $[M+H]^+$ | $C_{21}H_{20}O_{11}$ | 449, 287 | Kaempferol-3-*O* glucoside | Previously reported in *C. acutum* | [66, 67] |
| Positive | 6.69 | 449.1071 | 449.1082 | −2.4 | $[M+H]^+$ | $C_{21}H_{20}O_{11}$ | 449 | Luteolin-6-C-glucoside (Isoorientin) | First report in *C. acutum* | [68] |
| Positive | 6.69 | 449.1071 | 449.1066 | 1.1 | $[M+H]^+$ | $C_{21}H_{20}O_{11}$ | 449, 287 | Maritimetin-6-*O*-glucoside | First report in *C. acutum* | [69] |
| Positive | 6.79 | 465.1008 | 465.1033 | −5.4 | $[M+H]^+$ | $C_{21}H_{20}O_{12}$ | 465, 369, 303 | Quercetin 3-*O*-galactoside (Hyperin) | Previously reported in *C. acutum* | [66, 70] |
| Positive | 6.79 | 465.1008 | 465.1033 | −5.4 | $[M+H]^+$ | $C_{21}H_{20}O_{12}$ | 465, 303 | Quercetin-4′-glucoside | First report in *C. acutum* | [71] |
| Positive | 6.79 | 465.1008 | 465.1028 | −4.3 | $[M]^+$ | $C_{21}H_{21}O_{12}^+$ | 465, 303 | Delphinidin-3-Glucoside | First report in *C. acutum* | [72] |
| Negative | 6.81 | 477.1014 | 477.1033 | −3.9 | $[M—H]^-$ | $C_{22}H_{22}O_{12}$ | 477, 314 | Isorhamnetin-3-glucoside | First report in *C. acutum* | [73, 74] |
| Positive | 7.28 | 287.0557 | 287.0556 | 0.3 | $[M+H]^+$ | $C_{15}H_{10}O_6$ | 287, 213 | Fisetin | First report in *C. acutum* | [75] |
| Positive | 7.28 | 287.0550 | 287.0536 | 4.9 | $[M+H]^+$ | $C_{15}H_{10}O_6$ | 287, 213, 153 | Kaempferol | Previously reported in *C. acutum* | [76, 77] |
| Positive | 7.53 | 479.1181 | 479.1190 | −1.9 | $[M]^+$ | $C_{22}H_{23}O_{12}^+$ | 317, 302 | Petunidin-3-*O*-*β*-glucopyranoside | First report in *C. acutum* | [78] |
| Positive | 7.99 | 146.0602 | 146.0606 | −2.7 | $[M+H]^+$ | $C_9H_7NO$ | 118 | 3-formylindole | First report in *C. acutum* | [79, 80] |
| Positive | 8.91 | 137.0597 | 137.0603 | −4.4 | $[M+H]^+$ | $C_8H_8O_2$ | 137, 109, 95 | 4-acetylphenol | Previously reported in *C. acutum* | [81] |
| Negative | 9.76 | 271.0622 | 271.0606 | 5.9 | $[M—H]^-$ | $C_{15}H_{12}O_5$ | 271, 151, 119 | Naringenin | Previously reported in *C. acutum* | [82] |

**Table 1** (continued)

| Polarity Mode | Ret. Time (Min.) | Observed *m/z* | Calculated *m/z* | Mass Error (ppm) | Adduct | Molecular formula | MS/MS spectrum | Deduced compound | Occurrence in *C. acutum* | References |
|---|---|---|---|---|---|---|---|---|---|---|
| Negative | 10.53 | 299.0565 | 299.0556 | 3.0 | $[M—H]^-$ | $C_{16}H_{12}O_6$ | 299, 284, 256 | Kaempferide | First report in *C. acutum* | [51] |
| Positive | 11.19 | 301.0695 | 301.0712 | −5.6 | $[M+H]^+$ | $C_{16}H_{12}O_6$ | 301, 286 | | First report in *C. acutum* | [83] |
| Positive | 11.19 | 301.0685 | 301.0701 | −5.3 | $[M+H]^+$ | $C_{16}H_{12}O_6$ | 301.1, 286, 258.0 | Diosmetin | First report in *C. acutum* | [84] |

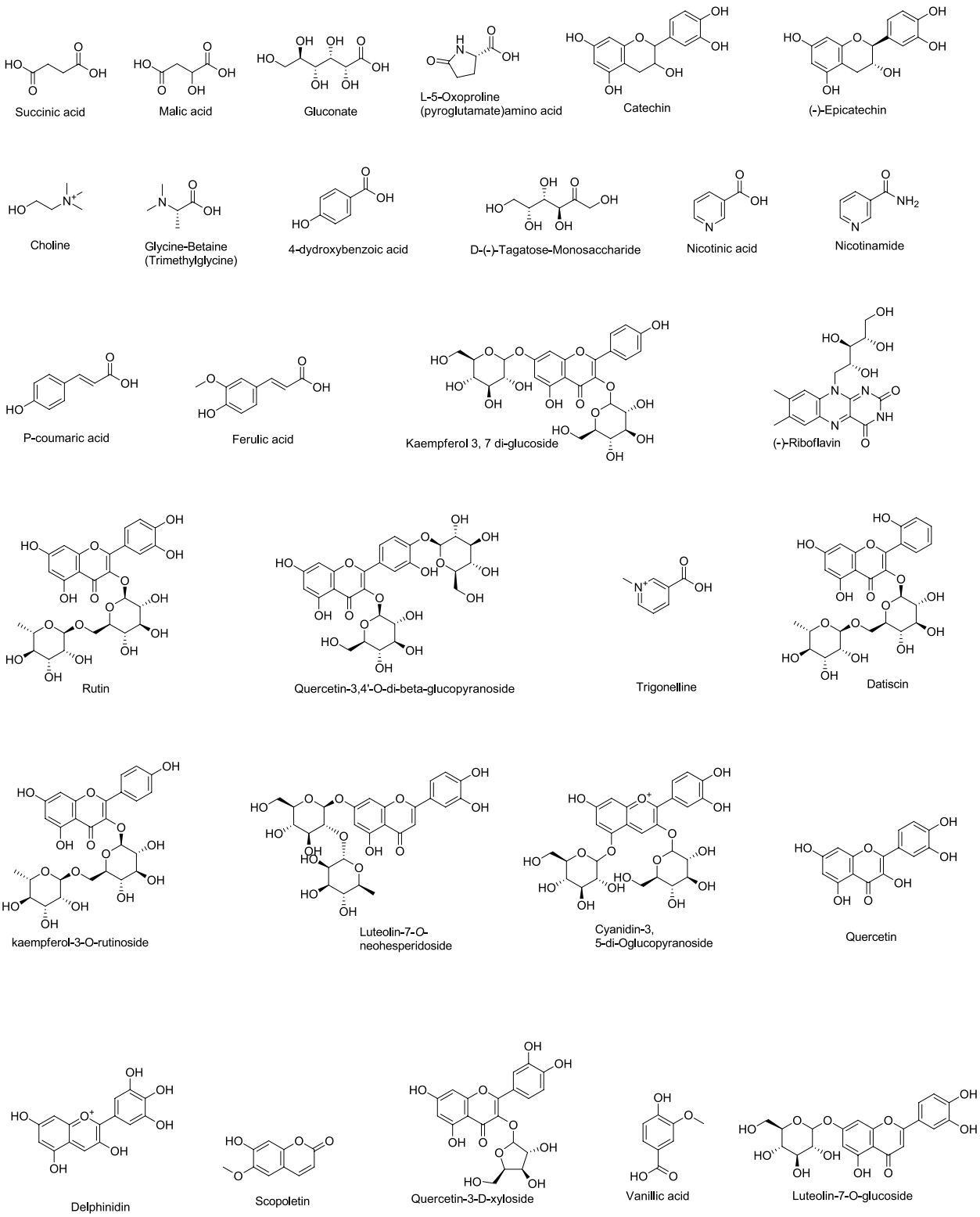
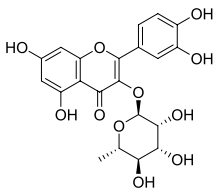
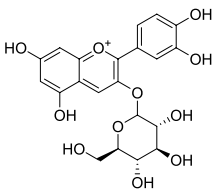
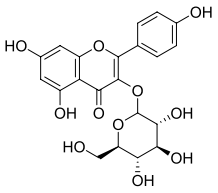
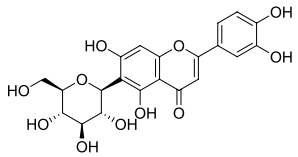


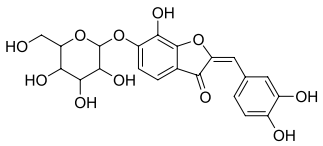

**Fig. 2** Chemical structure of identified compounds in *Cynanchum acutum* extract through LC–MS/MS

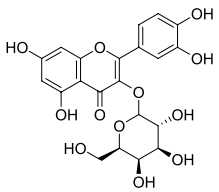

Quercetrin

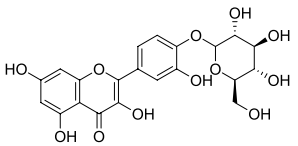

Cyanidin-3-glucoside

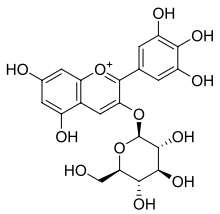

Kaempferol-3-O glucoside

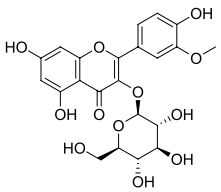

Luteolin-6-C-glucoside (Isoorientin)

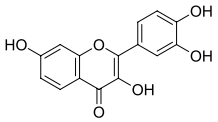

Maritimetin-6-O-glucoside

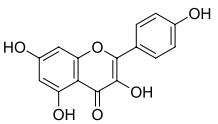

Quercetin 3-O-galactoside
Hyperin

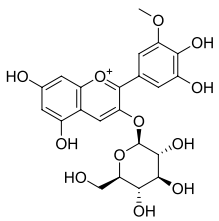

Quercetin-4'-glucoside

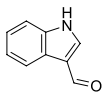

Delphinidin-3-glucoside

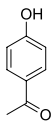

Isorhamnetin-3-glucoside

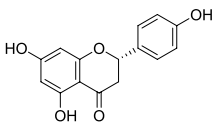

Fisetin

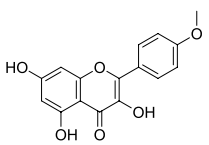

Kaempferol


Petunidin-3-O-beta-glucopyranoside


3-formylindole


4-acetylphenol


Naringenin


Kaempferide

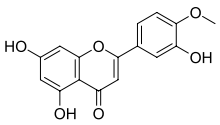

Diosmetin

**Fig. 2** continued

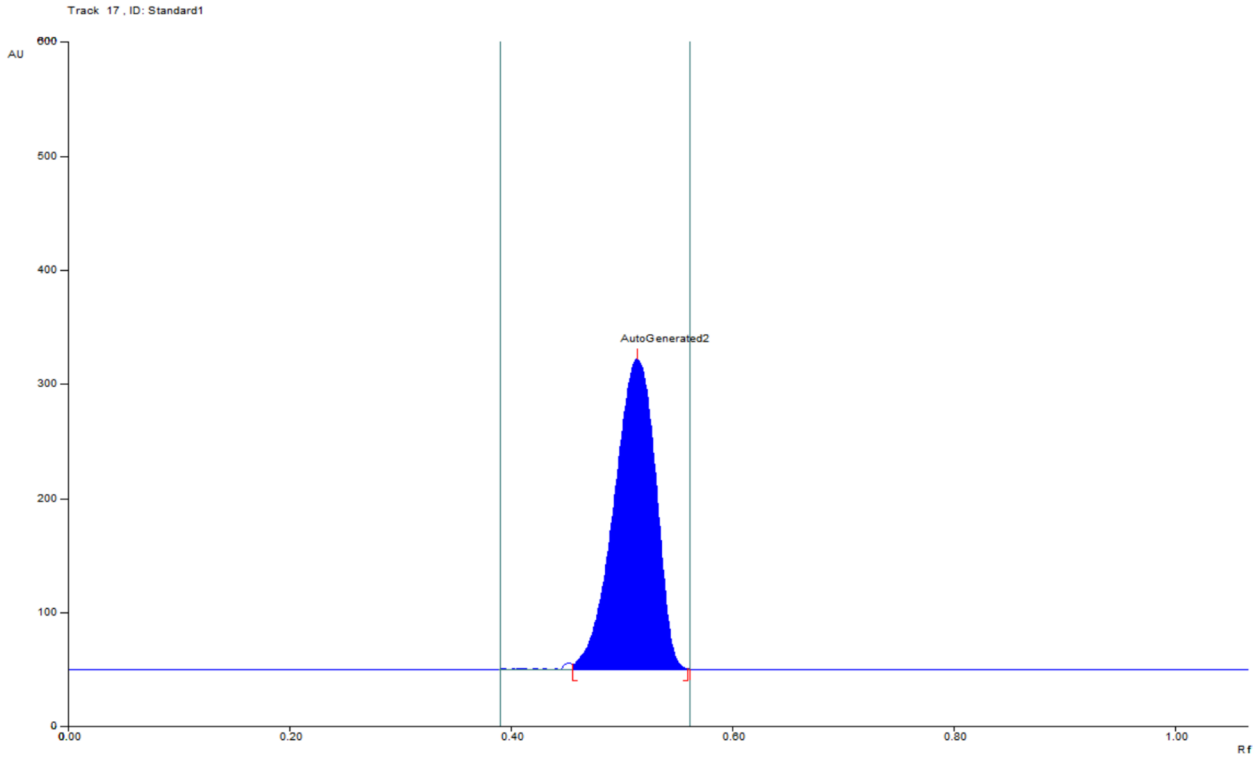



**Fig. 3** HPTLC Chromatogram of a single track of the standard quercetin-3-*O*-*β*-galactoside at 350 nm

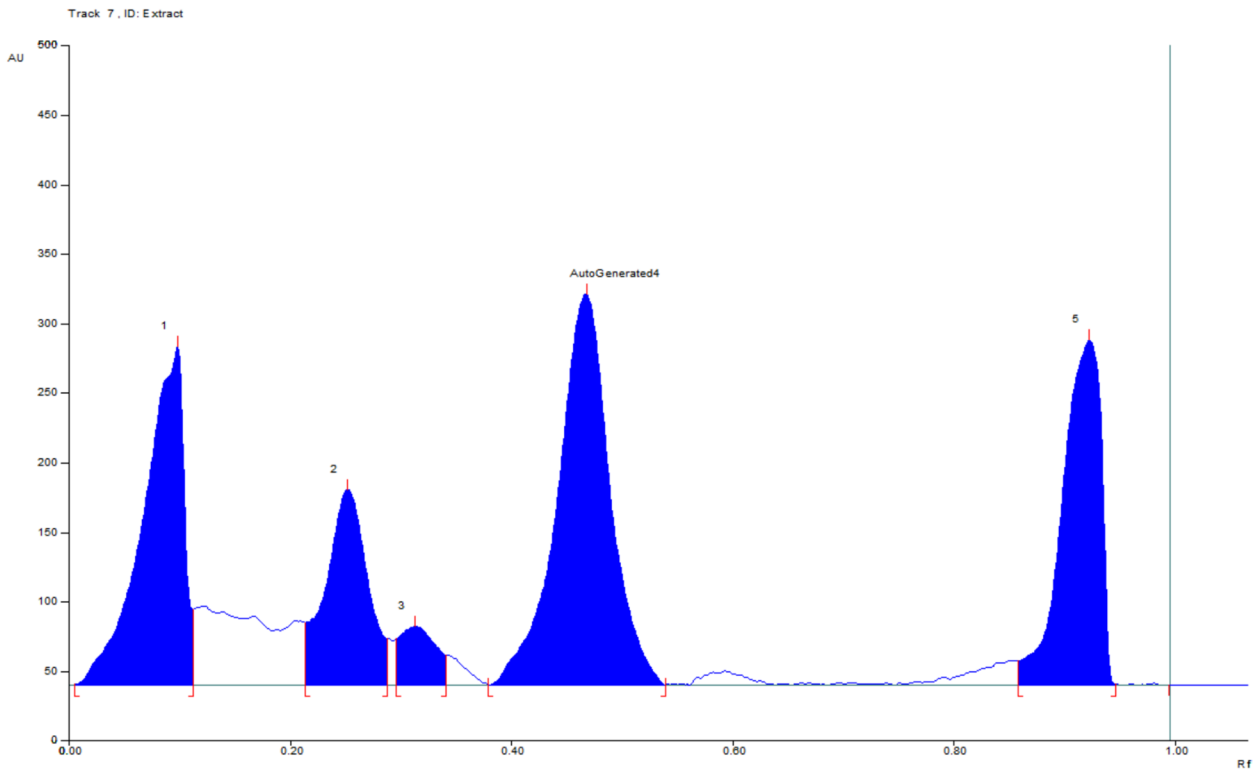



**Fig. 4** HPTLC Chromatogram of a single track of the crude extract of *C. acutum* at 350 nm

***Sample analysis***

The methodology proposed was applied for the quantification of quercetin-3-*O*-*β*-galactoside within the plant extract (Figs. 3, Fig. 4). The concentration was calculated based on the regression equation.

$$Y = 14.955X + 2342$$

Thus, the concentration was calculated to be 3.71 mg/1 g of the dry crude extract.

**Characterization of the semi-synthetic compounds (Q1 and Q2)**

The development of semi-synthetic analogues of bioactive constituents of medicinal herbs, including quercetin-3-*O*-*β*-galactoside, is a prevalent strategy employed in the drug discovery and development process. Structurally, quercetin-3-*O*-*β*-galactoside is a bioflavonoid having the privileged chromone scaffold with a 3′,4′ dihydroxyl phenyl ring on position 2, a galactosyl moiety on position 3, and hydroxyl groups on positions 5 and 7. This parent compound harbors high polar characteristics (predicted Log S = −3.04; solubility 0.423 mg/ml), the thing that would impose a significant penalty against its passage across cellular membranes as well as oral bioavailability low gastrointestinal (GI) bioavailability; SwissADME http://www.swissadme.ch/index.php). Masking polar groups through introducing hydrophobic moieties has been suggested as beneficial for providing a balanced hydrophilic/hydrophobic character to the parent compound, improving its respective kinetics. Thus, our strategy was to mask the OH group of the Quercetin-3-*O*-*β*-galactoside using different hydrophobic moieties through simple and straightforward nucleophilic substitution reactions to provide relevant semi-synthetic analogs of better physiochemical properties. Generally, quercetin-3-*O*-*β*-galactoside possesses four different aromatic hydroxyl groups. Nonetheless, the hydroxyl group on position 7 could be the most sterically vulnerable as well as the resonance-stabilized group for deprotonation and the subsequent nucleophilic substitution reactions.

The synthetic procedures for the preparation of the two semi-synthetic analogues are illustrated in Fig. 5. The first derivative was synthesized through the reaction of quercetin-3-*O*-*β*-galactoside with benzyl bromide in the presence of potassium carbonate under reflux. The benzyl-based product (Q1) was confirmed by the presence of the additional proton signals at 7.33–7.63 (m, 7 H) within the aromatic region as well as the relevant proton signal at 5.26 (d, *J* = 6.60 Hz, 2 H) due

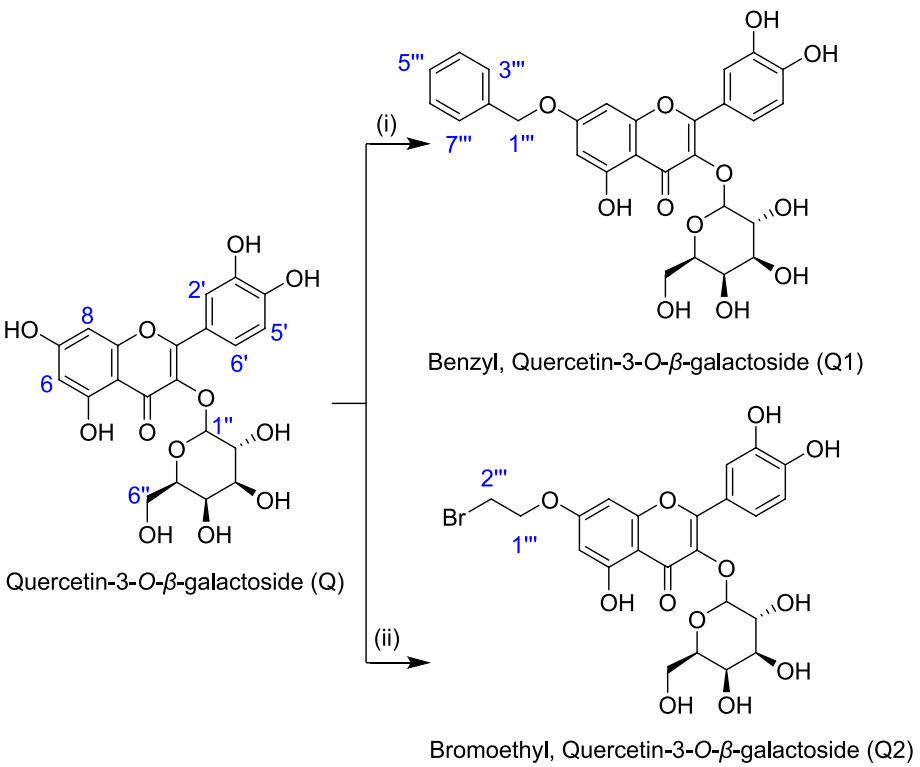



**Fig. 5** Synthesis of quercetin-3-*O*-*β*-galactoside derivatives (Q1-Q2); reagents and conditions: i) potassium carbonate, benzyl bromide, dry DMF, reflux, 12 h, yield: 85%; ii) 1-bromo-2-chloroethane, NaH, dry DMF, room temperature, Yield: 83%

to the newly attached benzyl side chain to the 7-OH through the methylene bridge (1‴ H) in the 1H-NMR spectrum. The second derivative was formed by the reaction of quercetin-3-*O*-*β*-galactoside with 1-bromo-2-chloroethane in the presence of sodium hydride as a reducing agent. The aliphatic-derived analog (Q2) was assured by presence of proton signals of the ethyl group at ~ 3.98 (m, 2 H), 4.31 (m, 2 H) due to the newly attached bromo ethyl side chain.

#### Assessment of in vitro biological activity of *Cynanchum acutum* extract and its semi-synthetic formula.

In vitro cell culture demonstrated the methanolic crude extract of *C. acutum* (sample 1) and the synthetic benzyl derivative of quercetin-3-*O*-*β*-galactoside (Q1- sample 3) with the highest antiviral activity against SARS-CoV-2 among the tested candidates, with $IC_{50}$ = 23.99 µg/mL, $CC_{50}$ = 327.9 µg/mL, and selectivity index (SI) = 13.66 for the crude methanolic extract and $IC_{50}$ = 29.21 µg/mL, $CC_{50}$ = 323.3 µg/mL, and SI = 11.06 for the synthetic benzyl derivative of quercetin-3-*O*-β-galactoside, compared to quercetin-3-*O*-*β*-galactoside (Q-sample 2), which exhibited $IC_{50}$ = 59.73 µg/mL, $CC_{50}$ = 368.3 µg/mL, and SI = 6.16. However, the synthetic bromo-ethyl derivative of quercetin-3-*O*-*β*-galactoside (Q2-sample 4) showed the lowest antiviral activity against SARS-CoV-2 with $IC_{50}$ = 91.16 µg/mL, $CC_{50}$ = 321.3 µg/mL, and SI = 3.42. Cytotoxicity and inhibition curves against SARS-CoV-2 in Vero E6 cells for the investigated compounds are shown in Fig. 6.

Interestingly, our LC–MS/MS analysis revealed C. *acutum* as a rich source of quercetin and quercetin analogues, which have been previously reported as powerful antiviral agents against different viruses via in

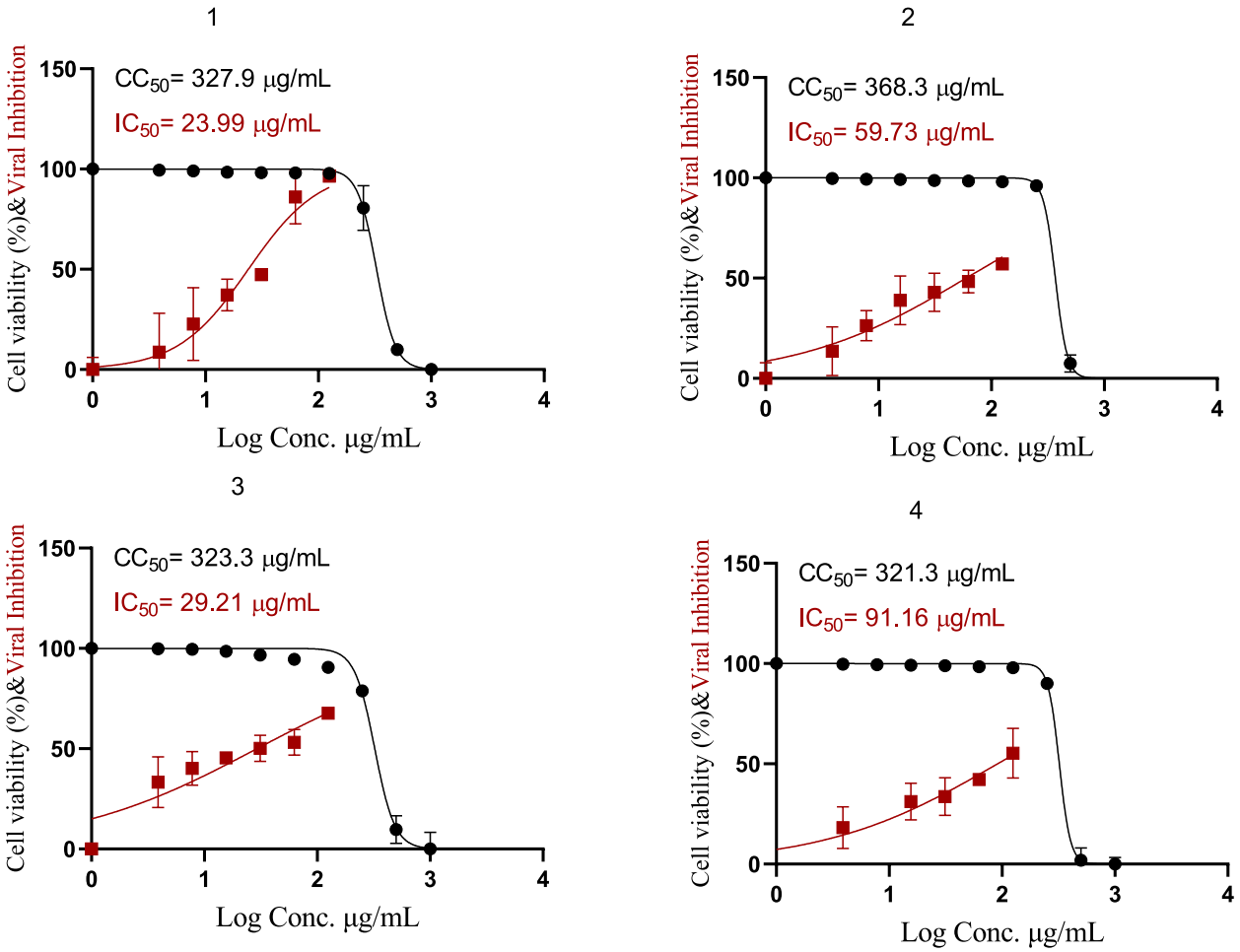



**Fig. 6** Cytotoxicity and inhibition curves against SARS-CoV-2 in Vero E6 cells for the methanolic crude extract of *Cynancum acutum* (Sample-1), quercetin-3-O-β-galactoside (Sample-2), benzyl derivative of quercetin-3-O-β-galactoside (Sample-3), and bromo-ethyl derivative of quercetin-3-O-β-galactoside (Sample-4), respectively. Using GraphPad Prism Software (version 8.02), cytotoxic concentration ($CC_{50}$) and inhibitory concentration 50% ($IC_{50}$) values were calculated by nonlinear regression analysis through plotting log inhibition against normalized response (variable slope). Error bars indicate standard deviation of five replicates

silico, in vitro, and in vivo approaches [21, 85, 86]. This explains the highest antiviral activity of the crude extract (Sample 1) against SARS-CoV-2 compared to other tested compounds in this study. However, promising comparable antiviral action was demonstrated for the synthetic benzyl derivative of quercetin-3-*O*-*β*-galactoside (Q1-Sample 3), highlighting the potential of the quercetin backbone as a scaffold for developing anti-SARS-CoV-2 agents. Among the most common flavonoids found in consumable fruits, vegetables, and traditional medicinal plants, quercetin stands out. Research has demonstrated that quercetin and its analogues possess different pharmacological characters, including the ability to combat viruses such as SARS-CoV-2 [21, 87]. In concordance, [88] demonstrated that quercetin weakly inhibits SARS-CoV-2 in Vero cells, whereas potent inhibition was observed for its synthetic derivative 8-(*P*-tolylselenyl)-quercetin in reverse transcription polymerase chain reaction (RT-PCR) assays. The same was true for [89], who showed quercetin, kaempferol, fisetin, and myricetin in plaque reduction assays to effectively inhibit SARS-CoV-2 in the epithelial cells of human lung (Calu-3).

### Docking analysis

Molecular modeling simulation highlighted the relevant anchoring of the small molecules investigated at the SARS-CoV-2 main protease (Mpro). Typically, the viral target protein enzyme (Mpro) is a cysteine protease homodimer consisting of two monomers/protomers designated A and B. Each protomer is composed of three distinct domains: domain I (residues 8–101), domain II (residues 102–184), and domain III (residues 201–306) [90]. The catalytic dyad, Cysteine amino acid and Histidine amino acid (Cys145 and His41), is situated within the gap between domains I and II, while domain III is predominantly made up of α-helices and responsible for regulation of the catalytic process [90]. The interface between the N-terminus of domains I and II and the C-terminus of domain III results in the creation of a reversible dimer in Mpro, which is further stabilized by the presence of substrate. It exerts its hydrolytic cleavage mechanism using the catalytic dyad of Cys145 and His41 residues.

The active site of SARS-CoV-2 Mpro is situated on each monomer at the cleft between domain I and II, while in its dimeric structure only a single catalytic site is functional [91]. The active site of Mpro can be categorized into six sub-pockets: S1′, S1, S2, S3, S4, and S5, where S1, S2, and S4 pockets are located within the protein cavity, but S1′, S3, and S5 are present on the upper surface of the protein [92]. The S1 region is defined by the side chains of various amino acid residues, including Phenylalanine amino acid (Phe140), His164, and Glutamic Acid (Glu166), while region S2 consists of hydrophobic amino acids such as Methionine amino acid (Met49) and (Met165). Regions S3 and S4 are significantly exposed to solvent and comprise amino acids like Alanine amino acid and Glycine amino acid (Ala191) and (Gly251).

Molecular docking investigations were conducted for the parent isolated compound (Q) as well as the two semi-synthetic small molecules (Q1 and Q2) into the active site of SARS-CoV-2 main protease. Initially, to ensure the reliability of the docking protocol, a re-docking procedure was executed for the co-crystallized ligand (piperazine-2-carboxamide derivative; reported $IC_{50} = 0.18$ μM [93]) into the active site of MPro with a binding score of -7.51 kcal/mol and aligned root-mean-square deviation (RMSD) = 1.10 Å. Achieving low re-docking RMSDs below 2.00 Å has been thoroughly reported as relevant for ensuring the validity of the adopted docking procedure for predicting binding modes and, in turn, binding energies with potential bioactivity significance [94, 95]. By analyzing docking results, all three compounds showed comparable orientation to that of the co-crystallized ligand at the Mpro active site with binding scores of -7.72, -8.34, and -7.22 kcal/mol for Q, Q1, and Q2, respectively. All docked compounds showed extended conformation/orientation across the different sub-pockets of the Mpro binding site. Notably, the binding energy scores of Q and Q1 surpassed that of the re-docked co-crystallized inhibitor, suggesting highly preferential binding affinity and anticipated enzyme inhibitory activity as well.

Regarding the binding interaction toward the Mpro pocket residues, Q1 interacted with the catalytic dyad Cys145 and His41 through hydrogen bonds and Pi-H

**Table 2** Receptor interactions and binding energies of all tested compounds (1 – 3) and the docked co-crystallized ligand at the Mpro binding Site

| Compound | S score | Rmsd | Amino acid interaction | Distance (A) |
|---|---|---|---|---|
| Q | −7.72 | 0.98 | His41 / H-bond<br>Asn142 / H-bond<br>Ser144 / H-bond | 2.1<br>3.3<br>2.6 &2.3 |
| Q1 | −8.34 | 1.18 | Cys145 / H-bond<br>Arg188 / H-bond<br>Gln189 / H-bond<br>Glu166 / pi-H bond<br>His41/ pi-H bond | 2.2<br>2.2<br>1.8<br>4.0<br>4.1 |
| Q2 | −7.22 | 1.30 | His41/ H-bond<br>Asn142/ H-bond<br>Arg188/ H-bond<br>Glu166/ H bond | 2.5<br>2.9<br>2.5<br>2.5 |
| Co-crystallized ligand | −7.51 | 1.1 | Gly143/ H-bond<br>Cys145/ H-bond<br>Glu166/ H-bond<br>Gln189/ H-bond | 1.8<br>1.9<br>1.9<br>2.0 |

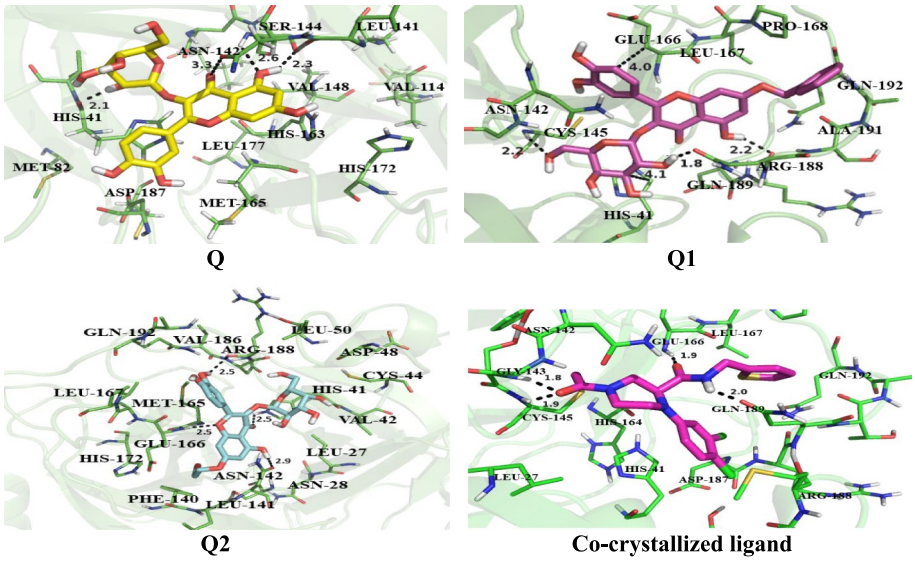



**Fig. 7** 3D-binding interactions of all docked compounds within the Mpro binding site (PDB: 8B56) as compared to the re-docked co-crystallized ligand. The enzyme is shown in a 3D cartoon representation, ligands are shown as sticks, and amino acids at 4 Å around the bound compounds are shown as lines. Polar interactions are illustrated as black-dashed lines

bonds, respectively, being proposed to be critical for small molecule inhibitory Mpro activity [93, 96]. Additional residue-wise interactions were observed with Arginine amino acid and Glutamine amino acid (Arg188) and (Gln189) (hydrogen bonds) and Glu166 (pi-H bond). Moving toward the Q-Mpro docked complex, several significant hydrogen bonds with His41 (one of the catalytic dyad residues), Asparagine amino acid (Asn142), and Serine amino acid (Ser144) residues were observed. Double hydrogen bond was assigned for the parent compound Q toward the His41 chains. The semi-synthetic analog, Q2, is also involved in several hydrogen bonds with His41, Asn142, Arg188, and Glu166 residues. The highlighted residue-wise interaction patterns were successfully translating the significant binding docking energies. Both (Table 2 and Fig. 7) illustrate the docking findings, including 3D binding modes, docking energies, RMSD values, and diverse interactions with the amino acids of the Mpro 256 pocket.

It is worth mentioning that the conducted molecular docking investigation primarily evaluates binding affinity and pose within the catalytic pocket of a particular biotarget; as an example here, the Mpro of SARS-CoV2. The conducted molecular docking investigation has been greatly rationalized to explore the potential mechanistic aspects of the tested compounds for having promising in vitro anti-SARS-CoV2 activity [97]. While compounds, like Q2, can exhibit relevant Mpro affinity despite their fair in vitro activity, which may be attributed to several factors, including cell permeability, compound stability in biological conditions, and potential off-target effects or metabolic liabilities. These are not fully captured by docking studies, where the latter do not account for pharmacokinetic properties that critically influence biological outcomes [98]. Therefore, we would like to emphasize that although docking can provide useful preliminary insights into potential target engagement, the observed biological activity reflects a more complex interplay of molecular and cellular factors that warrants further investigation.

## Conclusions

The *C. acutum* extract seems to exhibit valuable health benefits primarily due to its rich content of flavonoids. It could be useful as an herbal remedy to combat COVID-19 in its early mild stages. The synthetic benzyl derivative of quercetin-3-*O*-*β*-galactoside demonstrated promising anti-SARS-CoV2 activity. Molecular modeling findings revealed strong affinity and specific binding interactions for this compound at the MPro active site. Further experimental validation regarding the mechanistic aspects and compound's structural optimization process would be useful for pacing up the drug discovery and development pipeline of safe, nature-based SARS-CoV2 small molecule inhibitors.

### Abbreviations

| | |
|---|---|
| *%RSD* | Percent relative standard deviation |
| $^{13}$C NMR | Carbon nuclear magnetic resonance |
| $^{1}$H NMR | Proton nuclear magnetic resonance |
| Ala | Alanine amino acid |

| | |
|---|---|
| AMBER | Assisted model building with energy refinement |
| Arg | Arginine amino acid |
| Asn | Asparagine amino acid |
| C. acutum | Cynanchum acutum |
| Calu-3 | Human lung adenocarcinoma epithelial cells |
| $CC_{50}$ | 50% Cytotoxic concentration |
| CPE | Cytopathic effect |
| Cys | Cysteine amino acid |
| $ddH_2O$ | Double-distilled water |
| DMEM | Dulbecco's modified Eagle's medium |
| DMF | Dimethylformamide |
| DMSO | Dimethyl sulfoxide |
| DMSO-$d_6$ | Hexadeuterodimethyl sulfoxide |
| EUA | Emergency Use Authorization |
| FBS | Fetal Bovine Serum |
| FDA | Food and Drug Administration |
| GI | Gastrointestinal. |
| Gln | Glutamine amino acid |
| Glu | Glutamic acid |
| Gly | Glycine amino acid |
| hCoV-19 | Human Coronavirus-19 |
| His | Histidine amino acid |
| HPLC | High-performance liquid chromatography |
| HPTLC | High-performance thin-layer chromatography |
| $IC_{50}$ | 50% Inhibitory Concentration |
| ICH | International Council on Harmonization |
| LOD | Limit of detection |
| LOQ | Limit of quantification |
| Met | Methionine amino acid. |
| MOI | Multiplicity of infection |
| Mpro | Main protease (3-chymotrypsin-like protease) |
| MP-WS | Mobile phase working solution |
| MTT assay | (3-(4, 5-Dimethylthiazol-2-yl)-2, 5-diphenyltetrazolium bromide) cell viability assay |
| PBS | Phosphate-buffered saline |
| PDB | Protein Data Bank. |
| PDBQT | Protein Data Bank, Partial charge (Q) & Atom type (T) |
| pen/strep | Penicillin/Streptomycin |
| Phe | Phenylalanine amino acid |
| ppm | Part per million |
| RCSB | Research Collaboratory for Structural Bioinformatics |
| Rf | Retention factor |
| RMSD | Root-mean-square deviation |
| rpm | Revolutions per minute |
| RT-PCR | Reverse transcription polymerase chain reaction |
| SARS-CoV-2 | Severe acute respiratory syndrome coronavirus 2 |
| Ser | Serine amino acid |
| SI | Selectivity index |
| TIC | Total ion chromatogram |
| TLC | Thin-layer chromatography. |
| WHO | World Health Organization |

## Supplementary Information

The online version contains supplementary material available at https://doi.org/10.1186/s43094-025-00907-2.

Additional file1

**Acknowledgements**
This project was funded by the Deanship of Scientific Research (DSR) at King Abdulaziz University (KAU), Jeddah, Saudi Arabia, under grant number: (GPIP-1625-249-2024). The authors, therefore, acknowledge with thanks DSR for technical and financial support. The simulations in this work were performed at King Abdulaziz University's High Performance Computing Center (Aziz Supercomputer) (https://hpc.kau.edu.sa). The authors, therefore, acknowledge with thanks the center for technical support.

**Author contributions**
R.F.A.A. and S.S.E. suggested the research topic, investigated the article, investigated the article and participated in data representation and article revising and editing. A.KH.I. investigated the article, planned the research methodology, wrote the original draft, and participated in data representation and article revising and editing. K.M.D. and A.A.N. suggested the docking topic, investigated the article and participated in data representation and article revising and editing. A.M.A. suggested the semi-synthetic topic, investigated the article and participated in writing the original draft, S.S. suggested the antiviral topic, investigated the article and participated in writing the original draft. A.K.I. and S.S.A.M. suggested the research topic, planned the research methodology. M.O.L., A.A.N. and S.S.A.M. participated in revising and editing. S.A.A. suggested the research topic, planned the research methodology and participated in revising and editing. J.M.B. and S.S.E. suggested the research topic, planned the research methodology and participated in revising and editing. E.S.H., M.O.L. and M.T.I. investigated the article and participated in data representation.

**Funding**
This project was funded by the Deanship of Scientific Research (DSR) at King Abdulaziz University (KAU), Jeddah, Saudi Arabia, under grant number: (GPIP-1625–249-2024). The authors, therefore, acknowledge with thanks DSR for technical and financial support.

**Data availability**
All the data are available in the manuscript and further data could be given by the authors upon request.

## Declarations

**Ethics approval and consent to participate**
The study protocol was approved by the ethical committee of the Faculty of Pharmacy at Suez Canal University (approval number: 202010M2).

**Competing interests**
The authors declare that they have no competing interests.

**Author details**
[1]Department of Pharmacognosy, Faculty of Pharmacy, Suez Canal University, Ismailia 41522, Egypt. [2]Department of Pharmacognosy, Faculty of Pharmacy, Galala University, New Galala City, Suez 43713, Egypt. [3]Department of Medicinal Chemistry, Faculty of Pharmacy, Galala University, New Galala City, Suez 43713, Egypt. [4]Department of Medicinal Chemistry, Faculty of Pharmacy, Suez Canal University, Ismailia 41522, Egypt. [5]Department of Pharmaceutical Chemistry, Faculty of Pharmacy, Badr University in Cairo (BUC), Badr City, Cairo, P.O. 11829, Egypt. [6]Department of Microbiology and Immunology, Faculty of Pharmacy, Suez Canal University, Ismailia 41522, Egypt. [7]Department of Nursing College, North Private College of Nursing, Arar 73244, Saudi Arabia. [8]Department of Pharmaceutical Chemistry, Faculty of Pharmacy, King Abdulaziz University, Jeddah 21589, Saudi Arabia. [9]Department of Natural Products and Alternative Medicine, Faculty of Pharmacy, King Abdulaziz University, Jeddah 21589, Saudi Arabia. [10]Department of Pharmacy Practice, Faculty of Pharmacy, King Abdulaziz University, Jeddah 21589, Saudi Arabia. [11]Department of Biological Sciences, Faculty of Science, King Abdulaziz University, Jeddah 21589, Saudi Arabia.

Received: 11 July 2025 Accepted: 21 October 2025
Published: 30 October 2025

**References**

1. Wang HX, Ng TB (1999) Natural products with hypoglycemic, hypotensive, hypocholesterolemic, antiatherosclerotic and antithrombotic activities. Life Sci 65:2663–2677
2. Täckholm V (1974) Students' flora of Egypt, 2nd Cairo University, Egypt 888
3. Boulos L (2000) Flora of Egypt VII Al Hadara Publishing Cairo, Egypt
4. Fawzy GA, Abdallah HM, Marzouk MSA, Soliman FM, Sleem AA (2008) Antidiabetic and antioxidant activities of major flavonoids of *Cynanchum*

*acutum* L. (Asclepiadaceae) growing in Egypt. Z Naturforsch C 63:658–662
5. Youssef A, El-Swaify Z, Al-saraireh Y, Dalain S (2018) Cytotoxic activity of methanol extract of *Cynanchum acutum* L. seeds on human cancer cell lines. Latin Am J Pharm 37:1997–2003
6. Awaad A (2000) Phytochemical and biological activities of *Cynanchum acutum* growing in Egypt. Bull Fac Pharm Cairo Univ 38:153–162
7. AbouZeid AHS, Ibrahim NA, Sammour EA (2001) Phytochemical, insecticidal and molluscicidal investigations of the aerial parts of *Cynanchum acutum* L. growing in Egypt. Bull Fac Pharm Cairo Univ 39:235–245
8. El-Meligy RM, Zain ME, Ahmed FA (2014) Protective role of *Cynanchum acutum* L. extracts on carbon tetrachloride-induced hepatotoxicity in rat. Int J Chem Appl Biol Sci 1:9
9. Yan Y, Zhang J-X, Liu K-X, Huang T, Yan C, Huang L-J et al (2014) Seco-pregnane steroidal glycosides from the roots of *Cynanchum atratum* and their anti-TMV activity. Fitoterapia 97:50–63
10. Kim W, Oh T-S, Park Y-J (2017) Anti-viral effect of herbal medicine Korean traditional *Cynanchum paniculatum* (BGE.) kitag extracts. Afr J Tradit Complement Altern Med 14:194–198
11. Zhao Y-B, Shen Y-M, He H-P, Li Y-M, Mu Q-Z, Hao X-J (2004) Carbohydrates from *Cynanchum otophyllum*. Carbohydr Res 339:1967–1972
12. Konda Y, Iguchi M, Harigaya Y, Takayanagi H, Ogura H, Li X et al (1990) Hancokinol, a novel triterpene, from *Cynanchum hancokianum*. Tetrahedron Lett 31:5315–5318
13. Ahmed FH, Ka E (1990) Lupeol long-chain fatty acid esters and other lipid constituents from *cynanchum actum* L fam asclepiadaceae
14. Ge Yang, G. Y., Liu PingPing, L. P., Yang Rui, Y. R., Zhang Liu, Z. L., Chen HongXing, C. H., Camara, I. *et al.* (2015) Insecticidal constituents and activity of alkaloids from *Cynanchum mongolicum*
15. El-Demerdash A, Dawidar AM, Keshk EM, Abdel-Mogib M (2009) Coumarins from *Cynanchum acutum*. Rev Latinoam Quim 37:65–69
16. Heneidak S, Grayer RJ, Kite GC, Simmonds MSJ (2006) Flavonoid glycosides from Egyptian species of the tribe *Asclepiadeae* (Apocynaceae, subfamily Asclepiadoideae). Biochem Syst Ecol 34:575–584
17. Cai J, Zhang H, Zhu K, Zhu F, Wang Y, Wang S et al (2024) Risk of reinfection and severity with the predominant BA. 5 Omicron subvariant China, from December 2022 to January 2023. Emerg Microbes Infect 13:2292071
18. Higdon MM, Wahl B, Jones CB, Rosen JG, Truelove SA, Baidya A et al (2022) A systematic review of coronavirus disease 2019 vaccine efficacy and effectiveness against severe acute respiratory syndrome coronavirus 2 infection and disease. Open Forum Infect Dis. https://doi.org/10.1093/ofid/ofac138
19. Administration, U. S. F. a. D. (2023) Coronavirus (COVID-19) drugs in date last updated, https://www.fda.gov/drugs/emergency-preparedness-drugs/coronavirus-covid-19-drugs,
20. Araf Y, Akter F, Tang Yd, Fatemi R, Parvez MSA, Zheng C et al (2022) Omicron variant of SARS-CoV-2: genomics, transmissibility, and responses to current COVID-19 vaccines. J Med Virol 94:1825–1832
21. Dinda B, Dinda M, Dinda S, Ghosh PS, Das SK (2024) Anti-SARS-CoV-2, antioxidant and immunomodulatory potential of dietary flavonol quercetin: focus on molecular targets and clinical efficacy. Eur J Med Chem Rep 10:100125
22. Abdelhameed RFA, Ibrahim AK, Elfaky MA, Habib ES, Mahamed MI, Mehanna ET et al (2021) Antioxidant and anti-inflammatory activity of *Cynanchum acutum* L. isolated flavonoids using experimentally induced type 2 diabetes mellitus: biological and in silico investigation for nf-κb pathway/mir-146a expression modulation. Antioxidants 10:1713
23. Eltamany EE, Nafie MS, Khodeer DM, El-Tanahy AHH, Abdel-Kader MS, Badr JM et al (2020) *Rubia tinctorum* root extracts: chemical profile and management of type II diabetes mellitus. RSC Adv 10:24159–24168
24. Branch SK (2005) Guidelines from the international conference on harmonisation (ICH). J Pharm Biomed Anal 38:798–805
25. Sharma N, Sharma UK, Gupta AP, Sinha AK (2010) Simultaneous determination of epicatechin, syringic acid, quercetin-3-O-galactoside and quercitrin in the leaves of Rhododendron species by using a validated HPTLC method. J Food Compos Anal 23:214–219
26. Mostafa A, Kandeil A, Amm Elshaier Y, Kutkat O, Moatasim Y, Rashad AA et al (2020) FDA-approved drugs with potent in vitro antiviral activity against severe acute respiratory syndrome coronavirus 2. Pharmaceuticals 13:443
27. Eberhardt J, Santos-Martins D, Tillack AF, Forli S (2021) Autodock vina 1.2. 0: new docking methods, expanded force field, and python bindings. J Chem Inf Model 61:3891–3898
28. Yildiz I, Sen O, Erenler R, Demirtas I, Behcet L (2017) Bioactivity–guided isolation of flavonoids from *Cynanchum acutum* L. subsp. *sibiricum* (willd.) Rech. f. and investigation of their antiproliferative activity. Nat Prod Res 31:2629–2633
29. Chen ZS, Lai JS, Kao YH (1991) The constituents of *Cynanchum taiwanianum*. J Chin Chem Soc 38:393–396
30. Han L, Zhou X, Yang M, Zhou L, Deng X, Wei S et al (2018) Ethnobotany, phytochemistry and pharmacological effects of plants in genus *Cynanchum* Linn. (Asclepiadaceae). Molecules 23:1194
31. Gammatantrawet N, Nguyễn CT, Susawaengsup C, Ramli ANM, Tongkoom K, Chatsungnoen T et al (2025) Phytochemistry of medicinal herbs belongs to asclepiadaceae family for therapeutic applications: a critical review. Mol Biotechnol 67:885–909
32. Al Kadhi O, Melchini A, Mithen R, Saha S (2017) Development of a LC-MS/MS method for the simultaneous detection of tricarboxylic acid cycle intermediates in a range of biological matrices. J Anal Methods Chem 2017(1):5391832
33. Fernández-Fernández R, López-Martínez JC, Romero-González R, Martínez-Vidal JL, Alarcón Flores MI, Garrido Frenich A (2010) Simple LC–MS determination of citric and malic acids in fruits and vegetables. Chromatographia 72:55–62
34. Fiori J, Amadesi E, Fanelli F, Tropeano CV, Rugolo M, Gotti R (2018) Cellular and mitochondrial determination of low molecular mass organic acids by LC–MS/MS. J Pharm Biomed Anal 150:33–38
35. de Bois Maquillé L, Wund P, Renaudin L, Gautier C, Jardy A, Vial J et al (2015) Determination of gluconate in nuclear waste by high-performance liquid chromatography: comparison of pulsed amperometric detection and electrospray mass spectrometry detection. J Radioanal Nuclear Chem 306:213–220
36. Geenen S, Guallar-Hoyas C, Michopoulos F, Kenna JG, Kolaja KL, Westerhoff HV et al (2011) HPLC–MS/MS methods for the quantitative analysis of 5-oxoproline (pyroglutamate) in rat plasma and hepatic cell line culture medium. J Pharm Biomed Anal 56:655–663
37. Cai RJ, Yin XL, Liu J, Zhao GZ (2017) Characterization and identification of in vitro metabolites of (-)-epicatechin using ultra-high performance liquid chromatography-mass spectrometry. Trop J Pharm Res 16:2985–2990
38. Stöggl WM, Huck CW, Bonn GK (2004) Structural elucidation of catechin and epicatechin in sorrel leaf extracts using liquid-chromatography coupled to diode array-, fluorescence-, and mass spectrometric detection. J Sep Sci 27:524–528
39. Bruce SJ, Guy PA, Rezzi S, Ross AB (2010) Quantitative measurement of betaine and free choline in plasma, cereals and cereal products by isotope dilution LC-MS/MS. J Agric Food Chem 58:2055–2061
40. MacKinnon SL, Craft C (2015) Analysis of betaines from marine algae using LC-MS-MS natural products from marine algae: methods and protocols 267–275
41. Ali A, Bashmil YM, Cottrell JJ, Suleria HAR, Dunshea FR (2021) Lc-ms/ms-qtof screening and identification of phenolic compounds from Australian grown herbs and their antioxidant potential. Antioxidants 10:1770
42. Cocuron J-C, Ross Z, Alonso AP (2020) Liquid chromatography tandem mass spectrometry quantification of 13C-labeling in sugars. Metabolites 10(1):30
43. Lang R, Yagar EF, Eggers R, Hofmann T (2008) Quantitative investigation of trigonelline, nicotinic acid, and nicotinamide in foods, urine, and plasma by means of LC-MS/MS and stable isotope dilution analysis. J Agric Food Chem 56:11114–11121
44. Inamadugu JK, Damaramadugu R, Mullangi R, Ponneri V (2010) Simultaneous determination of niacin and its metabolites—nicotinamide, nicotinuric acid and N-methyl-2-pyridone-5-carboxamide—in human plasma by LC-MS/MS and its application to a human pharmacokinetic study. Biomed Chromatogr 24:1059–1074
45. Fang N, Yu S, Prior RL (2002) LC/MS/MS characterization of phenolic constituents in dried plums. J Agric Food Chem 50:3579–3585

46. Razgonova M, Zakharenko A, Pikula K, Manakov Y, ErcİŞLİ S, Derbush I et al (2021) LC-MS/MS Screening of phenolic compounds in wild and cultivated grapes *vitis amurensis* rupr. Molecules 26(12):3650
47. Sun J, Xiao Z, Lin L-Z, Lester GE, Wang Q, Harnly JM et al (2013) Profiling polyphenols in five *Brassica* species microgreens by UHPLC-PDA-ESI/HRMS n. J Agric Food Chem 61:10960–10970
48. Flieger M, Bandouchova H, Cerny J, Chudíčková M, Kolarik M, Kovacova V et al (2016) Vitamin B2 as a virulence factor in *Pseudogymnoascus destructans* skin infection. Sci Rep 6:33200
49. Lin Y, Xu W, Huang M, Xu W, Li H, Ye M et al (2015) Qualitative and quantitative analysis of phenolic acids, flavonoids and iridoid glycosides in Yinhua Kanggan tablet by UPLC-QqQ-MS/MS. Molecules 20:12209–12228
50. Abdel-Hamed AR, Mehanna ET, Hazem RM, Badr JM, Abo-Elmatty DM, Abdel-Kader MS et al (2021) Plicosepalus acacia extract and its major constituents, methyl gallate and quercetin, potentiate therapeutic angiogenesis in diabetic hind limb ischemia: HPTLC quantification and LC-MS/MS metabolic profiling. Antioxidants 10:1701
51. El Sayed AM, Basam SM, El-Naggar E-MBA, Marzouk HS, El-Hawary S (2020) LC–MS/MS and GC–MS profiling as well as the antimicrobial effect of leaves of selected Yucca species introduced to Egypt. Sci Rep 10:17778
52. (MoNA), M. o. N. A. (2024) Quercetin-3,4′-O-di-beta-glucoside In date last updated, https://mona.fiehnlab.ucdavis.edu/spectra/browse?query=exists(compound.metaData.name:%27InChIKey%27%20and%20compound.metaData.value:%27RPVIQWDFJPYNJM-DEFKTLOSSA-N%27),
53. Tine Y, Yang Y, Renucci F, Costa J, Wélé A, Paolini J (2017) LC-MS/MS analysis of flavonoid compounds from *Zanthoxylum zanthoxyloides* extracts and their antioxidant activities. Nat Prod Commun 12:1934578X1701201213
54. Shahat AA, Abdel-Shafeek KA, Husseiny HA, Claeys M, Apers S, Pieters L (2006) A new flavonoid from *Carrichtera annua*. Nat Prod Sci 12:122–124
55. Salerno R, Casale F, Calandruccio C, Procopio A (2016) Characterization of flavonoids in *Citrus bergamia* (Bergamot) polyphenolic fraction by liquid chromatography–high resolution mass spectrometry (LC/HRMS). PharmaNutrition 4:S1–S7
56. Ling Y, Ren C, Mallery SR, Ugalde CM, Pei P, Saradhi UVRV et al (2009) A rapid and sensitive LC–MS/MS method for quantification of four anthocyanins and its application in a clinical pharmacology study of a bioadhesive black raspberry gel. J Chromatogr B 877:4027–4034
57. Scigelova M, Hornshaw M, Giannakopulos A, and Makarov A (2011) Fourier transform mass spectrometry *Molecular & Cellular Proteomics* **10**
58. Montoro P, Tuberoso CIG, Perrone A, Piacente S, Cabras P, Pizza C (2006) Characterisation by liquid chromatography-electrospray tandem mass spectrometry of anthocyanins in extracts of *Myrtus communis* L. berries used for the preparation of myrtle liqueur. J Chromatogr A 1112:232–240
59. Zhong B, Robinson NA, Warner RD, Barrow CJ, Dunshea FR, Suleria HAR (2020) LC-ESI-QTOF-MS/MS characterization of seaweed phenolics and their antioxidant potential. Mar Drugs 18:331
60. Engels C, Gräter D, Esquivel P, Jiménez VM, Gänzle MG, Schieber A (2012) Characterization of phenolic compounds in jocote (*Spondias purpurea* L.) peels by ultra high-performance liquid chromatography/electrospray ionization mass spectrometry. Food Res Int 46:557–562
61. Song H-P, Zhang H, Fu Y, Mo H-Y, Zhang M, Chen J et al (2014) Screening for selective inhibitors of xanthine oxidase from Flos Chrysanthemum using ultrafiltration LC–MS combined with enzyme channel blocking. J Chromatogr B 961:56–61
62. Wang L, Halquist MS, Sweet DH (2013) Simultaneous determination of gallic acid and gentisic acid in organic anion transporter expressing cells by liquid chromatography–tandem mass spectrometry. J Chromatogr B 937:91–96
63. Sánchez-Ilárduya MB, Sánchez-Fernández C, Viloria-Bernal M, López-Márquez DM, Berrueta LA, Gallo B et al (2012) Mass spectrometry fragmentation pattern of coloured flavanol-anthocyanin and anthocyanin-flavanol derivatives in aged red wines of Rioja. Aust J Grape Wine Res 18:203–214
64. Lopes-Lutz D, Dettmann J, Nimalaratne C, Schieber A (2010) Characterization and quantification of polyphenols in Amazon grape (*Pourouma cecropiifolia* Martius). Molecules 15:8543–8552
65. Mazzoni L, Giampieri F, Suarez JMA, Gasparrini M, Mezzetti B, Hernandez TYF et al (2019) Isolation of strawberry anthocyanin-rich fractions and their mechanisms of action against murine breast cancer cell lines. Food Funct 10:7103–7120
66. Olennikov DN, Chirikova NK, Kashchenko NI, Nikolaev VM, Kim S-W, Vennos C (2018) Bioactive phenolics of the genus *Artemisia* (Asteraceae): HPLC-DAD-ESI-TQ-MS/MS profile of the Siberian species and their inhibitory potential against α-amylase and α-glucosidase. Front Pharmacol 9:756
67. Jang GH, Kim HW, Lee MK, Jeong SY, Bak AR, Lee DJ et al (2018) Characterization and quantification of flavonoid glycosides in the *Prunus* genus by UPLC-DAD-QTOF/MS. Saudi J Biol Sci 25:1622–1631
68. Ferreira RO, de Carvalho Junior AR, da Silva TMG, Castro RN, da Silva TMS, de Carvalho MG (2014) Distribution of metabolites in galled and non-galled leaves of *Clusia lanceolata* and its antioxidant activity. Rev Bras 6:617–625
69. Sánchez-Rabaneda F, Jáuregui O, Lamuela-Raventós RM, Viladomat F, Bastida J, Codina C (2004) Qualitative analysis of phenolic compounds in apple pomace using liquid chromatography coupled to mass spectrometry in tandem mode. Rapid Commun Mass Spectrom 18:553–563
70. Islam NM, Yoo HH, Lee MW, Dong Ms, Park YI, Jeong HS et al (2008) Simultaneous quantitation of five flavonoid glycosides in herba Epimedii by high-performance liquid chromatography–tandem mass spectrometry. Phytochem Anal 19:71–77
71. Bonaccorsi P, Caristi C, Gargiulli C, Leuzzi U (2005) Flavonol glucoside profile of southern Italian red onion (*Allium cepa* L.). J Agric Food Chem 53:2733–2740
72. Giordano L, Coletta W, Rapisarda P, Donati MB, Rotilio D (2007) Development and validation of an LC-MS/MS analysis for simultaneous determination of delphinidin-3-glucoside, cyanidin-3-glucoside and cyanidin-3-(6-malonylglucoside) in human plasma and urine after blood orange juice administration. J Sep Sci 30:3127–3136
73. Cantos E, Espin JC, Tomás-Barberán FA (2002) Varietal differences among the polyphenol profiles of seven table grape cultivars studied by LC– DAD– MS– MS. J Agric Food Chem 50:5691–5696
74. Eltamany EE, Goda MS, Nafie MS, Abu-Elsaoud AM, Hareeri RH, Aldurdunji MM et al (2022) Comparative assessment of the antioxidant and anticancer activities of *Plicosepalus acacia* and *Plicosepalus curviflorus*: metabolomic profiling and in silico studies. Antioxidants. https://doi.org/10.3390/antiox11071249
75. Goda MS, Nafie MS, Awad BM, Abdel-Kader MS, Ibrahim AK, Badr JM et al (2021) In vitro and in vivo studies of anti-lung cancer activity of *Artemesia judaica* L. crude extract combined with LC-MS/MS metabolic profiling, docking simulation and HPLC-DAD quantification. Antioxidants 11:17
76. Tsimogiannis D, Samiotaki M, Panayotou G, Oreopoulou V (2007) Characterization of flavonoid subgroups and hydroxy substitution by HPLC-MS/MS. Molecules 12:593–606
77. Devaraj VC, Krishna BG, Viswanatha GL (2011) Simultaneous determination of quercetin, rutin and kaempferol in the leaf extracts of *Moringa oleifera* Lam. and *Raphinus sativus* Linn. by liquid chromatography-tandem mass spectrometry. Zhong xi yi jie he xue bao J Chin Integr Med 9:1022–1030
78. Shin SC, Lee S-J, Lee SJ, Chung JI, Bae DW, Kim ST et al (2009) Comparison of anthocyanin content in seed coats of black soybean [*Glycine max* (L.) Merr.] cultivars using liquid chromatography coupled to tandem mass spectrometry. Food Sci Biotechnol 18:1470–1475
79. Zhang D, Sun Y, Shi Y, Wu X, Jia Q, Chen K et al (2021) Four new indole alkaloids from the roots of *Isatis tinctoria*. Nat Prod Res 36:312–318
80. Revelou P-K, Kokotou MG, Constantinou-Kokotou V (2019) Identification of auxin metabolites in Brassicaceae by ultra-performance liquid chromatography coupled with high-resolution mass spectrometry. Molecules 24:2615
81. Allen F, Greiner R, Wishart D (2015) Competitive fragmentation modeling of ESI-MS/MS spectra for putative metabolite identification. Metabolomics 11:98–110
82. Šibul F, Orčić D, Berežni S, Anačkov G, Mimica-Dukić N (2020) HPLC–MS/MS profiling of wild-growing scentless chamomile. Acta Chromatogr 32:86–94
83. Farias LdS, Mendez ASL (2014) LC/ESI-MS method applied to characterization of flavonoids glycosides in *B. forficata* subsp. pruinosa. Quim Nova 37:483–486

84. Silvestro L, Tarcomnicu I, Dulea C, Attili NRBN, Ciuca V, Peru D et al (2013) Confirmation of diosmetin 3-O-glucuronide as major metabolite of diosmin in humans, using micro-liquid-chromatography–mass spectrometry and ion mobility mass spectrometry. Anal Bioanal Chem 405:8295–8310
85. Ho W-Y, Shen Z-h, Chen Y, Chen T-H, Lu X, Fu Y-S (2024) Therapeutic implications of quercetin and its derived-products in COVID-19 protection and prophylactic *Heliyon* **10**,
86. Agrawal PK, Agrawal C, Blunden G (2020) Quercetin: antiviral significance and possible COVID-19 integrative considerations. Nat Prod Commun 15:1934578X20976293
87. Dabeek WM, Marra MV (2019) Dietary quercetin and kaempferol: bioavailability and potential cardiovascular-related bioactivity in humans. Nutrients 11:2288
88. Mangiavacchi F, Botwina P, Menichetti E, Bagnoli L, Rosati O, Marini F et al (2021) Seleno-functionalization of quercetin improves the non-covalent inhibition of Mpro and its antiviral activity in cells against SARS-CoV-2. Int J Mol Sci 22:7048
89. Chaves OA, Fintelman-Rodrigues N, Wang X, Sacramento CQ, Temerozo JR, Ferreira AC et al (2022) Commercially available flavonols are better SARS-CoV-2 inhibitors than isoflavone and flavones. Viruses 14:1458
90. Yang H, Yang M, Ding Y, Liu Y, Lou Z, Zhou Z et al (2003) The crystal structures of severe acute respiratory syndrome virus main protease and its complex with an inhibitor. Proc Natl Acad Sci U S A 100:13190–13195
91. Hu Q, Xiong Y, Zhu GH, Zhang YN, Zhang YW, Huang P et al (2022) The SARS-CoV-2 main protease (Mpro): structure, function, and emerging therapies for COVID-19. MedComm 3:e151
92. Kneller DW, Phillips G, Weiss KL, Pant S, Zhang Q, O'Neill HM et al (2020) Unusual zwitterionic catalytic site of SARS–CoV-2 main protease revealed by neutron crystallography. J Biol Chem 295:17365–17373
93. Gao S, Song L, Claff T, Woodson M, Sylvester K, Jing L et al (2022) Discovery and crystallographic studies of nonpeptidic piperazine derivatives as covalent SARS-CoV-2 main protease inhibitors. J Med Chem 65:16902–16917
94. Kontoyianni M, McClellan LM, Sokol GS (2004) Evaluation of docking performance: comparative data on docking algorithms. J Med Chem 47:558–565
95. El-Naggar AM, Hassan AMA, Elkaeed EB, Alesawy MS, Al-Karmalawy AA (2022) Design, synthesis, and SAR studies of novel 4-methoxyphenyl pyrazole and pyrimidine derivatives as potential dual tyrosine kinase inhibitors targeting both EGFR and VEGFR-2. Bioorg Chem 123:105770
96. Kronenberger T, Laufer SA, Pillaiyar T (2023) COVID-19 therapeutics: small-molecule drug development targeting SARS-CoV-2 main protease. Drug Discov Today 28:103579
97. Abd-Alla HI, Kutkat O, Sweelam H-T, Eldehna WM, Mostafa MA, Ibrahim MT, Moatasim Y, GabAllah M, Al-Karmalawy AA (2022) Investigating the potential anti-SARS-CoV-2 and anti-MERS-CoV activities of Yellow necklacepod among three selected medicinal plants: extraction, isolation, identification, in vitro, modes of action, and molecular docking studies. Metabolites 12(11):1109
98. Bajpai M, Esmay JD (2002) In vitro studies in drug discovery and development: an analysis of study objectives and application of good laboratory practices (GLP). Drug Metab Rev 34(4):679–689

## Publisher's Note

Springer Nature remains neutral with regard to jurisdictional claims in published maps and institutional affiliations.